HOKKAIDO UNIVERSITY

Title	Studies on neuronal function using votage-gated Ca2+ channel Cav2.1α1 subunit mutant mice
Author(s)	金, 泰延
Degree Grantor	北海道大学
Degree Name	博士(獣医学)
Dissertation Number	乙第6998号
Issue Date	2016-09-26
DOI	https://doi.org/10.14943/doctoral.r6998
Doc URL	https://hdl.handle.net/2115/63575
Type	doctoral thesis
File Information	Tae_Yeon_Kim.pdf

Hokkaido University Collection of Scholarly and Academic Papers : HUSCAP

Studies on neuronal function using voltage-gated Ca^{2+} channel $Cav2.1\alpha_1$ subunit mutant mice

(Cav2.1チャネルの神経機能における役割に関する研究

－ Cav2.1α1遺伝子変異マウスを用いて－)

Tae Yeon Kim

Table of Contents

General Introduction **1**

Chapter 1. Protective effect of a Cav2.1 channel in kainate-induced seizure and neuronal injury of *rolling Nagoya* mice **6**

1. Introduction **7**

2. Materials and methods **9**

2.1. Animals 9

2.2. *In situ* hybridization (ISH) 9

2.3. Real-time quantitative reverse transcription polymerase chain reaction (qRT-PCR) analysis 10

2.4. Seizure assessment based on behavioral analysis 11

2.5. Histopathology 12

2.6. Quantification of neuronal degeneration 13

2.7. Western blot analysis 13

2.8. Statistical analyses 14

3. Results **15**

3.1. Expression patterns of Cav2.1α_1 and kainate/AMPA receptor in the hippocampus 15

3.2. Decreased sensitivity of aged *rol*/+ mice to kainate-induced seizures 17

3.3. Reduced kainate-induced neuronal damage in aged *rol*/+ mice 19

3.4. Low activity of p38 MAPK in the hippocampus of aged *rol*/+ mice after kainate injection 28

4. Discussion **30**

5. Summary **35**

Chapter 2. Protective effect of a Cav2.1 channel in cryogenic brain injury of *rolling Nagoya* mice....36

1. Introduction....37

2. Materials and methods....39

2.1. Animals....39

2.2. Cryogenic model preparation....39

2.3. Determination of lesion size....41

2.4. Drug application....41

2.5. Immunohistochemistry (IHC)....41

2.6. Quantification of neuronal degeneration....42

2.7. Western blot analysis....43

2.8. Statistical analyses....43

3. Results....44

3.1. Cryogenic brain injury-induced brain lesion area....44

3.2. Astrocyte proliferation following cryogenic brain injury....46

3.3. Reduction in neuronal damage following cryogenic brain injury....49

3.4. Therapeutic effect of ω-aga injection against cryogenic brain injury....52

3.5. pp38 expression in the ω-aga-treated +/+ mice after cryogenic brain injury55

4. Discussion....57

5. Summary....61

Chapter 3. Characterization of *tottering-6j* mice....62

1. Introduction....63

2. Materials and methods....65

2.1. Animals....65

2.2. ISH....65

2.3. Real-time qRT-PCR analysis 66
2.4. IHC 68
2.5. Quantification of Purkinje cells and granular cells 68
2.6. Cresyl violet and terminal deoxynucleotidyl transferase-mediated dUTP digoxigenin nick-end-labeling (TUNEL) stainings 69
2.7. Electroencephalograms (EEGs) and behavioral observations 69
2.8. Effects of antiepileptic drugs 70
2.9. Statistical analyses 71
3. Results 72
3.1. mRNA expression in *tottering-6j* mice. 72
3.2. Histopathological observation of gross morphology and protein expression patterns in the cerebellum of *tottering-6j* mice 75
3.3. Apoptotic cell death in the cerebellum of *tottering-6j* mice 78
3.4. Absence-like seizures of *tottering-6j* mice 79
3.5. Effects of antiepileptic drugs on absence-like seizures in *tottering-6j* mice 80
4. Discussion 81
5. Summary 87
General Conclusion 88
Summary 90
Acknowledgment 93
References 94
Summary in Japanese 107

Abbreviations

AMPA : α-amino-3-hydroxy-5- methyl-4-isoxazolepropionic acid

ANOVA : Analysis of variance

Calb1 : Calbindin D-28K

Calb2 : Calretinin

Cav2.1α_1 : α_1 subunit of Cav2.1 channel

CNS : Central nervous system

Ct value : Threshold cycle value

DAPI : 4',6-diamidino-2-phenylindole

EA2 : Episodic ataxia type 2

EEG : Electroencephalogram

ESM : Ethosuximide

FHM1 : Familiar hemiplegic migraine type 1

FJB : Fluoro Jade B

GABA : γ -amino butyric acid

GAPDH : Glyceraldehyde 3-phosphate dehydrogenase

GFAP : Glial fibrillary acidic protein

H&E : Hematoxylin and eosin

IHC : Immunohistochemistry

ISH : *In situ* hybridization

I.P. : Intraperitoneal

la : *leaner*

MAPK : Mitogen-activated protein kinase

NMDA : N-methyl-D-aspartate

PB : Phosphate buffer

PBS : Phosphate-buffered saline

PFA : Paraformaldehyde

PHT : Phenytoin

pp38 : phosphorylated p38 MAPK

qRT-PCR : Quantitative reverse transcription polymerase chain reaction

rol/*rol* : Homozygous *rolling Nagoya*

rol/+ : Heterozygous *rolling Nagoya*

rkr : *rocker*

Ryr1 : Ryanodine receptor 1

Ryr2 : Ryanodine receptor 2

Ryr3 : Ryanodine receptor 3

SCA6 : Spinocerebellar ataxia type 6

SEM : Standard errors of the mean

SWD : Spike-and-wave discharge

TBI : Traumatic brain injury

tg : *tottering*

TH : Tyrosine hydroxylase

TUNEL : Terminal deoxynucleotidyl transferase-mediated dUTP digoxigenin nick-end-labeling

VGCC : Voltage-gated Ca^{2+} channel

VPA : Valproic acid

Zebrin II : Zebrin II

ω-aga : ω-agatoxin IVA

ω-aga +/+ mice : ω-aga-pretreated +/+ mice

+/+ : Wild-type mice

General Introduction

Voltage-gated Ca^{2+} channels (VGCCs) are the proteins located on presynaptic terminals widespread in central nervous system (CNS) (Takahashi, 2012; Simms and Zamponi, 2014; Heyes S. et al., 2015). It is activated by depolarization and facilitates Ca^{2+} current and regulates intracellular processes such as neurotransmitter release, axonal outgrowth, membrane excitability and synaptic plasticity (Takahashi, 2012). Subtypes of high VGCCs including Cav1 (L-type), Cav2.1 (P/Q-type), Cav2.2 (N-type) and Cav2.3 (R-type) could be delineated on physiological and pharmacological bases. Each type has their antagonists such as ω-agatoxin IVA (ω-aga) for Cav2.1 (Table 1).

High VGCC is a molecular complex consisted of 4 subunits: α_1, α_2/δ, β, and γ (Catterall, 1998; Takahashi, 2012; Simms and Zamponi, 2014) (Fig. 1). α_1 subunits are the main pore-forming unit, encoded by a family of genes (*CACNA1A*, *CACNA1B*, *CACNA1C*, *CACNA1D*, *CACNA1E*, *CACNA1F*, *CACNA1G*, *CACNA1H*, *CACNA1I* and *CACNA1S*). α_1 subunits are essential for VGCC functions and properties, including voltage sensing and protein binding. (Catterall and Few, 2008; Catterall, 2011; Campiglio and Flucher, 2015). It has four homologous transmembrane domains (I–IV), each containing six membrane-spanning helices (S1–S6), plus a reentrant p-loop motif that lines the channel pore, enabling the passage of Ca^{2+} (Fig. 1). The four domains are connected through cytoplasmic linkers, and both the C- and N-termini are cytoplasmic and interact with regulatory proteins (Catterall and Few, 2008).

α_1 subunit of Cav2.1 channel (Cav2.1α_1) is encoded in *CACNA1A* gene. Mutations of this gene have been found in humans. It triggers a wide range of neurological symptoms and disorders including familiar hemiplegic migraine type 1 (FHM1),

episodic ataxia type 2 (EA2), spinocerebellar ataxia type 6 (SCA6), and epilepsy (Takahashi, 2012; Zamponi et al., 2015). Mutations in the Cav2.1α_1 gene were also have been seen in mice. Spontaneous mutant mice, having mutation in Cav2.1α_1 gene on chromosome 8, includes *rocker* (*rkr*), *tottering* (*tg*), *rolling Nagoya*, *tottering-4j*, *tottering-5j*, *tottering-6j* and *leaner* (*la*) mice (Fig. 2). These mice exhibit ataxia, and movement disorder (Takahashi, 2012).

The *rolling Nagoya* mouse is a natural mutant exhibiting ataxia and problem in balancing. It's mutation results in an amino acid change at R1262G in the voltage-sensing S4 segment located on domain 3 of Cav2.1α_1 (Mori et al., 2000). The Ca^{2+} current amplitude exhibits a 40% reduction in homozygous *rolling Nagoya* (*rol*/*rol*) compared to wild-type (+/+) control mice (Mori et al., 2000).

Glutamate is one of the most important excitatory neurotransmitter binds to 4 types of receptors; ionotropic glutamate, kainate, α-amino-3-hydroxy-5-methyl-4-isoxazolepropionic acid (AMPA), and N-methyl-D-aspartate (NMDA) receptors (Rojas and Dingledine, 2013). It is one of the systems regulated by Cav2.1 channel (Turner et al., 1992; Lee et al., 2009). Glutamate-induced excitotoxicity is now considered as mechanism of neuronal death in ischemia, CNS trauma and epilepsy (Rajendra et al., 2004). A study reported that by blocking Cav2.1 channel had protective effect against glutamate related brain injury, such as ischemia (Asakura et al., 1997; Tian et al., 2013). However, the effect of Cav2.1 channel in kainate-induced brain injury and traumatic brain injury (TBI) has not been investigated.

Another mutant mice, *tottering-6j* mice are chemically generated a recessive mutant strain, by the Neuroscience Mutagenesis Facility at The Jackson Laboratory, using ethylnitrosourea (Li et al., 2012). In *tottering-6j* mice, mutation in the Cav2.1α_1 gene results in a base substitution (C-to-A) in the consensus splice acceptor sequence,

which results in deletion of a part of the S4-S5 linker, S5, and a part of S5-S6 linker domain I in the Cav2.1α_1. These results show poor motor coordination. Since it is recently reported mutant mice, its seizure, pharmacological profile in epilepsy, and protein expression pattern in cerebellum are not investigated.

Under existing circumstances, the studies were focused on protective effect of Cav2.1 channel in glutamate related neuronal injuries using *rolling Nagoya* mice, and pharmacological and protein expression characteristic of new mutant mice, *tottering-6j* mice.

Table 1. Physiological function and pharmacology of Cav channel subtypes

Cav subtype	Antagonists	Physiological function
Cav1 (L-type)	Dihydropyridine Phenylalkylamines Benzothiazepines	Excitation-contraction coupling Calcium homeostasis Gene regulation Neurotransmitter release
Cav2.1 (P/Q-type)	ω-agatoxin IVA	Neurotransmitter release Dendritic Ca^{2+} transients Hormone release
Cav2.2 (N-type)	ω-conotoxin GVIA	Neurotransmitter release Dendritic Ca^{2+} transients Hormone release
Cav2.3 (R-type)	SNX-482	Repetitive firing Dendritic Ca^{2+} transients
Cav3 (T-type)	None	Pacemaking Repetitive firing

Table adapted from: Catterall et al., 2005

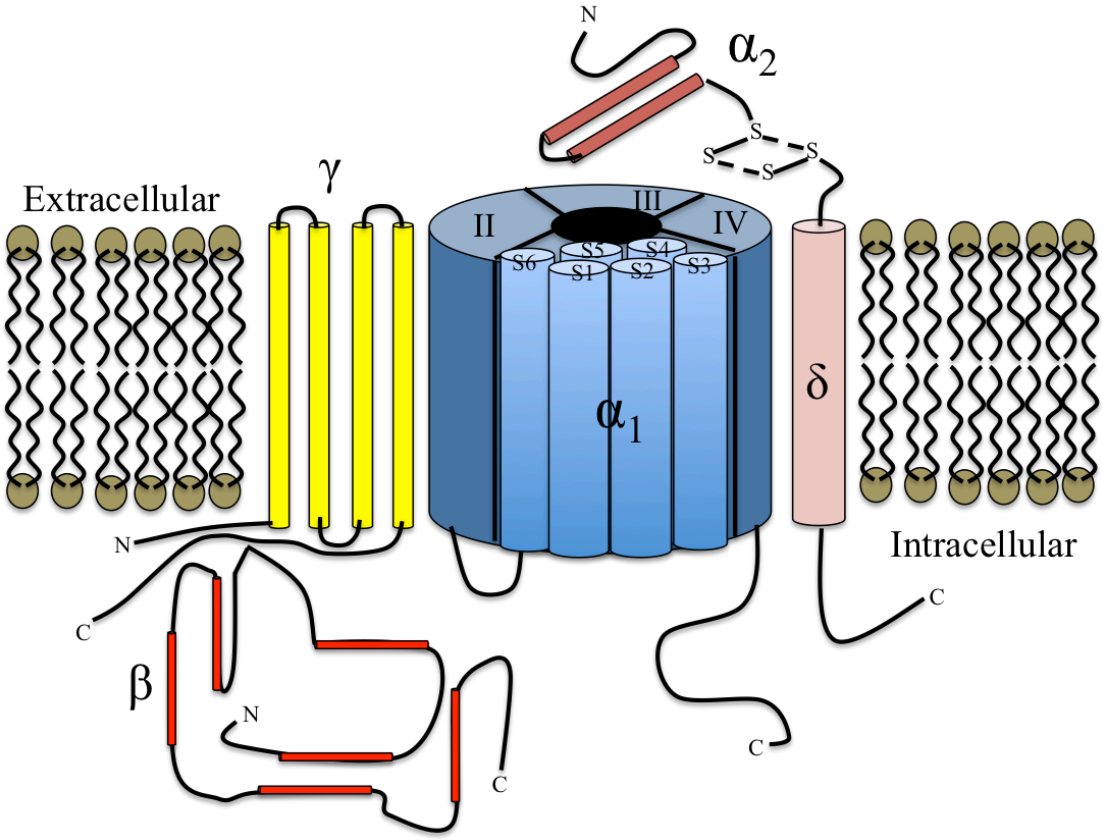

Fig.1. Structure of high VGCC. High VGCC is a molecular complex consisted of α_1, α_2/δ, β, and γ subunits. α_1 subunit is consisted of four homologous transmembrane domains (I–IV), each containing six membrane-spanning helices (S1–S6), and a reentrant p-loop motif that lines the channel pore, the four domains are connected through cytoplasmic linkers, and both the C- and N-termini are cytoplasmic.

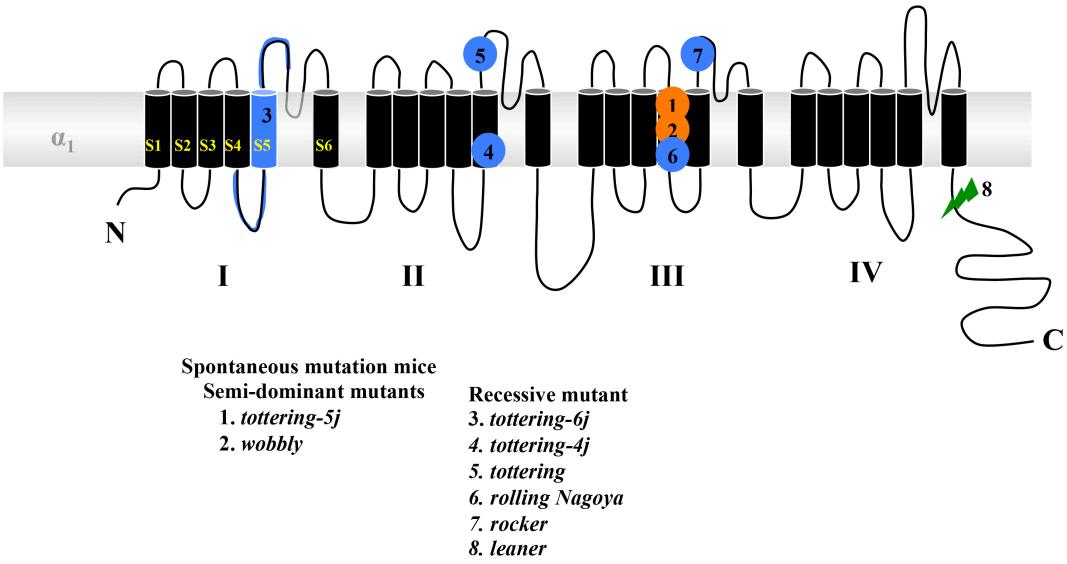

Fig. 2. Location of mouse mutations in the secondary structure of the Cav2.1α_1. *Tottering-5j* and *wobbly* mice are semi-dominant mutants and *tottering*, *rolling Nagoya*, *rocker*, *leaner*, *tottering-4j* and *tottering-6j*, are recessive mutants.

Chapter 1.

Protective effect of a Cav2.1 channel in kainate-induced seizure and neuronal injury of *rolling Nagoya* mice

1. Introduction

Epilepsy is a neuronal disease frequent in human regardless of age, gender and race. About 1% of the population is known to have epilepsy and it often requires lifelong medication (Hauser et al., 1993). Seizures could be divided in two groups: partial and generalized seizure. Generalized seizure could be grouped into symptomatic generalized epilepsy and idiopathic generalized epilepsy. Symptomatic generalized epilepsy is known to have a reason, such as infection or anoxia. On the other hand, idiopathic generalized epilepsy has no clear etiology and might be related at the genetic level withdrawal, such as mutation of Ca^{2+} channel (Leonardi and Ustun, 2002). Since Cav2.1 channel plays essential role in synaptic transmission, abnormality in Cav2.1 channel affects both cellular and network behavior, leading to neuronal disorder including epilepsy (Evans and Zamponi, 2006; Jarvis and Zamponi, 2007).

Glutamate is one of the most important excitatory neurotransmitter, which is coupled to glutamatergic system (Lee et al., 2009). It binds to postsynaptic glutamate receptors after released. There are 4 types of glutamate receptors, including kainate and AMPA receptors. Kainate directly binds to five subtypes of kainate receptor, such as GluK1 (Grik1), GluK2 (Grik2), GluK3 (Grik3), GluK4 (Grik4), and GluK5 (Grik5), and four subtypes of AMPA receptor, such as, GluA1 (Gria1), GluA2 (Gria2), GluA3 (Gria3), and GluA4 (Gria4) (Fukuta et al., 2005). Each receptor subunit is encoded by distinct gene. The overactivation of these receptors by excessive kainate evokes excitatory postsynaptic currents at hippocampal synapses closely related to epilepsy. Indeed, the administration of excessive kainate to animal subjects induces persistent spikes of high amplitude and frequency discharges

(Williams et al., 2006) and the resulting excitotoxicity can cause seizure and neuronal cell death (Watkins and Jane, 2006). Therefore, kainate injection is used as an experimental model to reveal the precise mechanism of excitotoxicity, and the kainate/AMPA receptors are an appropriate drug target for an antiepileptic drug (Contractor et al., 2011; Bassani et al., 2013; Faught, 2014).

The *rolling Nagoya* mouse has a mutation in the Cav2.1α_1 (Mori et al., 2000). *rol*/*rol* mice have been reported to exhibit ataxia but not seizures, after about 2 weeks of age (Oda, 1973). On the other hand, heterozygous *rolling Nagoya* (*rol*/+) mice have no apparent behavioral deficits at 2 months of age. However, systemic or intra-hippocampal injection of the NMDA receptor antagonist MK-801 decreased spatial cognition in 2-month-old *rol*/+ mice (Takahashi et al., 2010).

It has not been elucidated whether Cav2.1α_1 dysfunctions in *rol*/+ mice affect kainate-induced signaling leading to seizure and neuronal damage. Since *rol*/*rol* mice exhibit ataxia, it was not appropriate to evaluate seizure activity after kainate injection. In previous studies, male mice with C57BL/6 background were resistant to excitotoxin sensitivity when injected with kainate (McKhann et al., 2003; McCord et al., 2008). Female mice are more susceptible to kainate-induced excitotoxicity than males, similar to humans (Zhang et al., 2008). Therefore, female *rol*/+ mice were used based on this study.

This study was focused on the role of Cav2.1 in kainate-regulated excitotoxicity by using 2-month-old and 18-month-old female *rol*/+ mice. Kainate/AMPA receptor signaling-induced seizure and the number of neurodegenerated cells were examined. Also, differences in expression patterns of Cav2.1α_1, p38, one of the mitogen-activated protein kinases (MAPK) activated by kainate (Namiki et al., 2007); and phosphorylated p38 (pp38) were compared in the hippocampus.

2. Materials and methods

2.1. Animals

This research was conducted in accordance with the Declaration of Helsinki and was approved by the Animal Experiments Committee of the RIKEN Brain Science Institute (Approval ID: No. H26-2-204). All animals were cared for and treated humanely in accordance with the Institutional Guidelines for Experiments using Animals. Two-month-old (5- to 8-week-old) and 18-month-old (69- to 72-week-old) female *rol*/*rol*, *rol*/+, and +/+ mice with a C57BL/6 genetic background mice were used (Tian et al., 2013). Separate groups of female mice were used for each study. All of the mice were housed under environmental conditions of 21 ± 2°C, humidity of 55 ± 10%, lighting of 350 lux (at bench level) and a 12:12 light:dark cycle (light from 8:00 am to 8:00 pm). Animals were housed in microisolation cages (MBS7115RHMV, 19.1 × 29.2 × 12.7 cm, Allentown Inc., NJ, USA) with bedding (TEK-FRESH, Harlan Teklad, WI, USA) and given access to irradiated food (CRF-1; Oriental Yeast, Tokyo, Japan) and filtered water *ad libitum*. The health status of animals was monitored twice daily.

2.2. *In situ* hybridization (ISH)

The mice were anesthetized with pentobarbital sodium (Kyoritsuseiyaku Corporation, Tokyo, Japan) and were intracardially perfused with ice-cold 4% paraformaldehyde (PFA) in 0.1 M phosphate buffer (PB) (pH 7.4). Paraffin-embedded blocks and sections of mouse brain tissue for ISH were obtained from Genostaff Co. Ltd. (Tokyo, Japan). Each mouse brain was dissected after perfusion, fixed with tissue fixative (Gonostaff) and embedded in paraffin according to

proprietary procedures in 6 μm sections. The hybridization protocol was conducted as previously reported (Sakuraoka et al., 2012). The probe for a 504 bp cDNA fragment was designed from positions 3229 to 3732 of the Cav2.1α_1 cDNA and labeled with a digoxygenin RNA labeling kit (Roche Diagnostics, Mannhein, Germany). Coloring reactions were performed with NBT/BCIP solution (Sigma-Aldrich, MO, USA) overnight and washed with phosphate-buffered saline (PBS). The sections were counterstained with Kernechtrot stain solution (Mutoh Pure Chemicals, Tokyo, Japan) and mounted with CC/Mount (Diagnostic Biosystems Inc., CA, USA).

2.3. Real-time quantitative reverse transcription polymerase chain reaction (qRT-PCR) analysis

The mice were euthanized with an overdose of pentobarbital sodium. Total RNA was isolated from the hippocampus and liver using TRIzol reagent, according to the manufacturer's protocol (Invitrogen, CA, USA). To quantify the mRNA level of the gene of interest, qRT-PCR in duplicate assays was performed using an ABI7700 sequence detection system (Applied Biosystems, CA, USA), as previously described (Takahashi and Niimi, 2009). First-strand cDNA was synthesized from 1 μg total RNA using a TaqMan reverse transcription reagent system (Applied Biosystems). The primers and probes used to determine wild-type Cav2.1α_1 gene expression, mutant Cav2.1α_1 gene expression and the total amount of Cav2.1α_1 gene expression including both +/+ and mutant mice are described in a previous study (Takahashi and Niimi, 2009). The mRNA levels of kainate receptors (Grik1, Grik2, Grik3, Grik4, and Grik5) and AMPA receptors (Gria1, Gria2, Gria3, and Gria4) were measured using Applied Biosystems TaqMan Gene Expression Assays (Grik1, Assay ID Mm00446882_m1; Grik2, Assay ID Mm00599860_m1; Grik3, Assay ID Mm01179716_m1; Grik4,

Assay ID Mm00615472_m1; Grik5, Assay ID Mm00433774_m1; Gria1, Assay ID Mm00433753_m1; Gria2, Assay ID Mm00442822_m1; Gria3, Assay ID Mm00497506_m1; Gria4, Assay ID Mm00444754_m1). The 18S ribosomal RNA (Assay ID Hs99999901_s1, Applied Biosystems TaqMan Gene Expression Assay) was used for normalization. The PCR conditions were 94°C for 10 min, followed by 40 cycles at 95°C for 15 sec and 60°C for 1 min. All samples were analyzed in duplicate and the threshold cycle (Ct) value, which reflects the amount of PCR product, was calculated. The relative levels of expression were determined based on the Ct values after normalization to glyceraldehyde 3-phosphate dehydrogenase (GAPDH), a housekeeping gene. (Takahashi and Niimi, 2009).

2.4. Seizure assessment based on behavioral analysis

The mice with the C57BL/6 background were monitored continuously every 30 min for 3 hr to evaluate seizure activity after intraperitoneal (I.P.) injection of kainate (Sigma-Aldrich). The drug dose (20 mg/kg) was determined according to a previous report (Namiki et al., 2007). The test was conducted between 9:00 am and 4:00 pm by a well-trained experimenter who was blinded to the mouse strains. Seizure classification was as follows: score 1, mice became motionless after exploring, sniffing, and grooming ceased; score 2, forelimb and/or tail extension, giving the appearance of a rigid postural tone; score 3, myoclonic jerks of the head and neck, with brief twitching movements; score 4, forelimb clonus and partial rearing; score 5, forelimb clonus, rearing, and falling; score 6, generalized tonic-clonic activity with loss of postural tone, often resulting in death.

2.5. Histopathology

The mice were anesthetized with pentobarbital sodium and were intracardially perfused with ice-cold 4% PFA in 0.1 M PB (pH 7.4) 1 week after kainate or vehicle injection. Then the brains were removed, placed in fixative for 1 day, and cut coronally into samples 20 μm thick using a cryostat (Leica, Heidelberg, Germany). The sections were stained with hematoxylin and eosin (H&E) and double-stained with Fluoro-Jade B (FJB) (Chemicon, CA, USA) and anti-glial fibrillary acidic protein (GFAP) (1:500; Cy3-labeled anti-GFAP, Millipore Corporation, MA, USA). To assess the severity and extent of neurodegeneration in the CA1 and CA3 regions of the hippocampus according to H&E staining, sections were scored using a semiquantitative grading system: score 1, normal; score 2, slight shrinkage of neurons (1–4% pyknotic neurons in CA1 or CA3); score 3, moderate shrinkage of neurons (5–15% pyknotic neurons in CA1 or CA3); score 4, severe shrinkage of neurons (more than 15% pyknotic neurons in CA1 or CA3); score 5, slight loss of neurons (5–10% neuronal loss in CA1 or CA3); score 6, moderate loss of neurons (11–40% neuronal loss in area CA3); and score 7, severe loss of neurons (more than 40% neuronal loss in CA1 or CA3). Mean values of pathological changes in both sides of the hippocampus were calculated for each mouse. Immunostained slides were observed using a conventional fluorescence microscope (IX81, Olympus, Tokyo, Japan) and a digital camera (CoolSNAP™ HQ, Roper Industries, GA, USA) incorporating a charge-coupled device. FJB is an anionic fluorescein derivative that is useful for histological staining of neurons undergoing degeneration. Upregulation of GFAP is a consistent pathological feature in neurodegenerative diseases. 4',6-diamidino-2-phenylindole (DAPI) (DAPI-Fluoromount-G™; Southern Biotech, AL, USA) was used as a nuclear counterstain. To assess positive cells in the CA1 and CA3 regions of

the hippocampus, sections were rated independently by two observers using a semiquantitative scale: baseline staining (−), mild response (+), moderate response (++), and intense response (+++). The criteria used for each scale was defined by Colburn et al. (1997).

2.6. Quantification of neuronal degeneration

The numbers of FJB-positive cells were counted in defined areas of the CA1 and CA3 regions in a blinded manner in sections that were double-stained with DAPI and FJB. All subfields were counted and the numbers for each side were averaged into single values for each animal. Six square counting frames (400 × 400 μm^2) were randomly placed in the pyramidal layers of the CA1 and CA3 regions of the four regularly spaced coronal sections from each animal.

2.7. Western blot analysis

Experiments were performed according to a previous report (Niimi et al., 2008). The mice were euthanized with an overdose of pentobarbital sodium 1 week after kainate or vehicle injection, and then decapitated. Brains were removed and washed in ice-cold saline for 1–2 min. The proteins from the hippocampus were extracted using PRO-PREP^{TM} Protein Extraction Solution (iNtRON Biotechnology Inc., Gyeonggi, Korea) according to the manufacturer's instructions. A 20 μg sample of each protein was electrophoresed on a 10% SDS-polyacrylamide gel and the bands were transferred to a polyvinylidene difluoride membrane (Immobilon-P, Millipore Corporation). Commercial rabbit polyclonal antibody specific for anti-p38 phosphorylated at threonine-180 and tyrosine-182 (1:500; Abcam, Cambridge, UK)

was used for immunodetection. The membranes were stripped in stripping buffer and reprobed with rabbit monoclonal anti-p38 antibody (1:500; Abcam). Then there were again stripped in stripping buffer and reprobed with mouse monoclonal β-actin antibody (1:250; Chemicon, CA, USA) as a control for protein loading. HRP-conjugated anti-rabbit IgG (1:25000; Jackson Immuno Research Lab. Inc., PA, USA) and HRP-conjugated anti-mouse IgG (1:50000; Jackson Immuno Research Lab. Inc.) were used as secondary antibodies. The blots were developed using an ECL Plus Western Blotting Detection System (GE Healthcare, NJ, USA). Protein signals were visualized and quantified using the ImageJ software. Protein bands were boxed and the integrated intensity of all pixels within the box was calculated against average background levels for a box of the same size. The amount of protein was normalized to β-actin.

2.8. Statistical analyses

The data are presented as the means ± standard errors of the mean (SEM). Statistical analyses were conducted using Excel Statistics 2006 (SSRI, Tokyo, Japan). The data were analyzed using a Dunnett's test or analysis of variance (ANOVA). Bonferroni post hoc comparisons between groups were performed when appropriate. The results were considered to be statistically significant at a $P < 0.05$ or lower probability of error.

3. Results

3.1. Expression patterns of Cav2.1α_1 and kainate/AMPA receptor in the hippocampus

The expression patterns of Cav2.1α_1 mRNA were assessed in the mouse hippocampus using ISH (2-month-old *rol*/+, +/+: n = 6 each; 18-month-old *rol*/+, +/+: n = 6 each) and real-time qRT-PCR analysis (2-month-old *rol*/*rol*, *rol*/+, +/+: n = 10 each; 18-month-old *rol*/*rol*, *rol*/+, +/+: n = 10 each). In the ISH using the antisense probe (Fig. 3, top), the Cav2.1α_1 expression patterns in the hippocampus with strong expression in the CA1 and CA3 regions of 2- and 18-month-old *rol*/+ mice did not differ compared to those of age-matched +/+ mice. There were no signals in any of the brains using the sense probe (data not shown). In real-time qRT-PCR analysis (Fig. 3, bottom), the total-type assay was not significantly different in the transcripts of Cav2.1α_1 in 2- or 18-month-old *rol*/+ or +/+ mice. The wild-type and total-type assays gave similar results for 2- and 18-month-old +/+ mice (data not shown). The mutant-type and total-type assays also gave similar results for 2- and 18-month-old *rol*/+ mice (data not shown). In 2-month-old *rol*/+ mice, more wild-type Cav2.1α_1 transcripts were expressed than mutant-type Cav2.1α_1. Conversely, in 18-month-old *rol*/+ mice, fewer wild-type Cav2.1α_1 transcripts were expressed than mutant-type transcripts. No products in real-time qRT-PCR analysis were observed in the hippocampus of +/+ mice in the mutant-type assay or in the hippocampus of *rol*/*rol* mice in the wild-type assay (data not shown). No products were observed in the liver fractions of all strains in the wild-type, mutant-type, and total-type assays (data not shown). In the hippocampus, the transcript levels of kainate receptors including Grik1, Grik2, Grik3, Grik4, and Grik5 and of AMPA receptors including Gria1, Gria2,

Gria3, and Gria4 did not differ significantly in 2- and 18-month-old rol/+ or +/+ mice (data not shown).

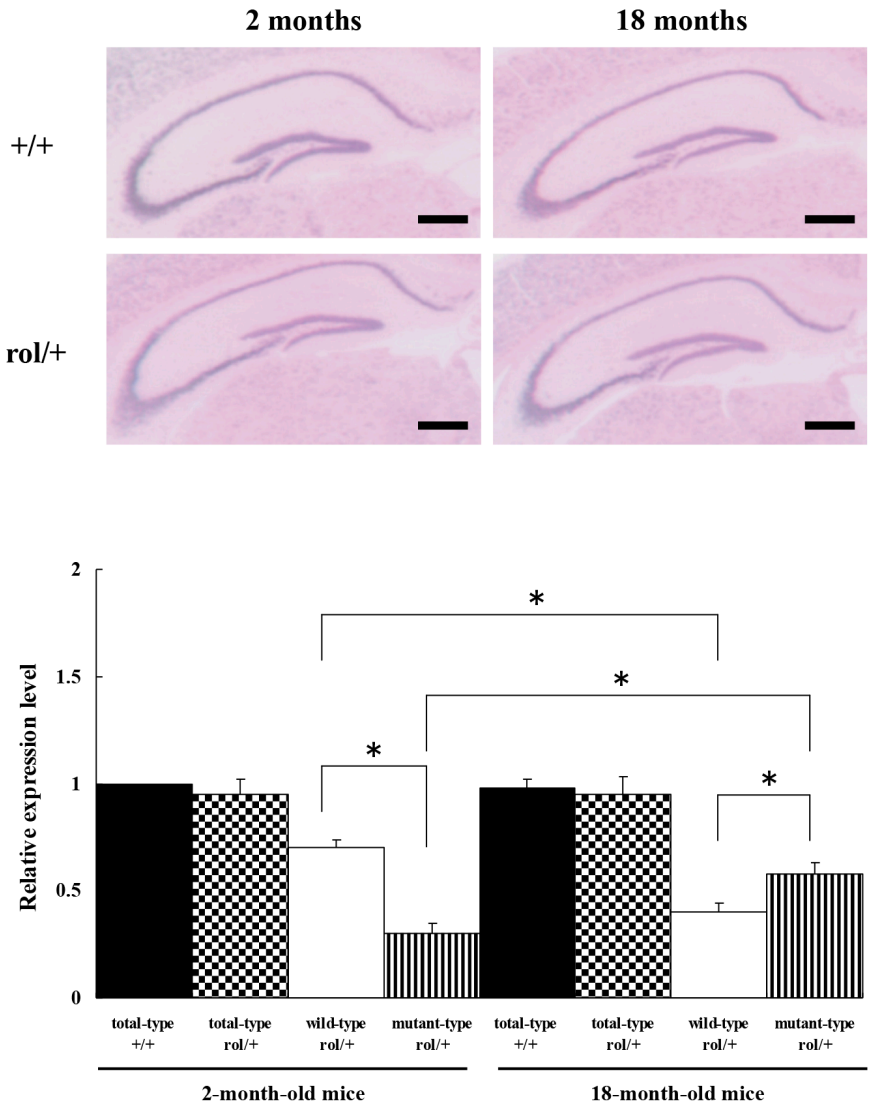

Fig. 3. Expression patterns of Cav2.1α$_1$ mRNA. Representative hippocampus sections of 2- and 18-month-old +/+ and *rol*/+ mice using ISH analysis (top). The expression patterns of total-type, wild-type, and mutant-type Cav2.1α$_1$ mRNA in the hippocampus of 2- and 18-month-old +/+ and *rol*/+ mice using real-time qRT-PCR analysis (bottom). The mRNA expression level for each type was calculated relative to wild-type Cav2.1α$_1$ mRNA expression in 2-month-old +/+ mice. Each bar represents 200 μm. * $P < 0.05$, compared to the appropriate control (Dunnett's test).

3.2. Decreased sensitivity of aged *rol*/+ mice to kainate-induced seizures

Kainate-injected 2-month-old (*rol*/+, +/+: n = 12 each) and kainate-injected 18-month-old (*rol*/+, +/+: n = 12 each) mice were used to examine sensitivity to kainate. As shown in Fig. 4, administration of kainate caused a significantly different maximum seizure score between *rol*/+ and +/+ mice [strain × age, $F(1,44) = 22.98$, $P < 0.01$]. Severity of seizure in 2-month-old *rol*/+ mice (maximum seizure score = 4.5 ± 0.23) was similar to that in age-matched +/+ mice (maximum seizure score = 4.6 ± 0.15) [$F(1,22) = 0.09$, $P > 0.05$]. In contrast, severity of seizure in 18-month-old *rol*/+ mice (maximum seizure score = 3.3 ± 0.33) was lower than that in age-matched +/+ mice (maximum seizure score = 5.4 ± 0.19) [$F(1,22) = 32.33$, $P < 0.01$]. The maximum seizure score observed in 18-month-old +/+ mice was higher than that in 2-month-old +/+ mice [$F(1,22) = 11.70$, $P < 0.01$].

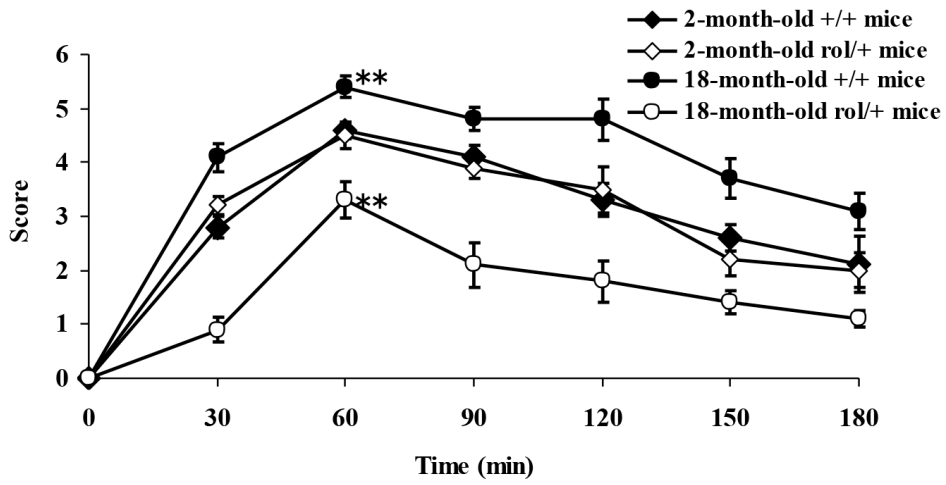

Fig. 4. Analysis of behavioral seizure score at 30 min intervals following kainate administration. At 60 min, differences in maximum seizure scores were observed among the groups. $^{**}P < 0.01$ when compared to the appropriate control (Bonferroni post hoc comparisons).

3.3. Reduced kainate-induced neuronal damage in aged *rol*/+ mice

Vehicle-injected 2-month-old (*rol*/+, +/+: n = 8 each), vehicle-injected 18-month-old (*rol*/+, +/+: n = 8 each), kainate-injected 2-month-old (*rol*/+, +/+: n = 8 each), and kainate-injected 18-month-old (*rol*/+, +/+: n = 8 each) mice were used to examine neuronal damage. H&E-stained hippocampus sections from *rol*/+ and +/+ mice were investigated 1 week after I.P. injection of kainate. As shown in Fig. 5, neuronal damage characterized by pyknotic nuclei, shrinkage, and spongy degeneration was found in the CA1 and CA3 regions of the hippocampus of 2-month-old *rol*/+ and +/+ mice and 18-month-old +/+ mice, and was not typically observed in the 18-month-old *rol*/+ mice. Because activated astrocytes are proliferative and highly immunoreactive to the anti-GFAP antibody, indicating neurodegeneration, how GFAP-positive cells appeared in the CA1 (Fig. 6, top) and CA3 (Fig. 7, top) regions of the hippocampus was elucidated where the neuronal damage and loss occurred. The results of the positively immunostained cells in the CA1 (Table 2) and CA3 (Table 3) regions were rated using a semiquantitative scale. A number of reactive astrocytes were observed in the CA1 and CA3 regions of the hippocampus of 2-month-old *rol*/+ and +/+ mice and 18-month-old +/+ mice 1 week after injection of kainate. Reactive astrocytes seemed to occur alongside the neuronal damage indicated by FJB in the CA1 (Fig. 6, Table 2) and CA3 (Fig. 7, Table 3) regions. In contrast, both reactive astrocytes and FJB-positive damaged neurons were rarely observed in the CA1 and CA3 regions of the hippocampus of 18-month-old *rol*/+ mice 1 week after kainate injection. In the CA1 (Fig. 6I) and CA3 (Fig. 7I) regions, GFAP-positive cells were barely detected in vehicle-injected 18-month-old +/+ mice. The numbers of FJB-positive damaged neurons were counted in the CA1 (Fig. 6, bottom) and CA3 regions (Fig. 7, bottom) of 2-month-old *rol*/+ and +/+ mice and 18-month-old *rol*/+ and +/+ mice 1 week after

kainate injection. Indeed, the number of FJB-positive cells in the CA1 and CA3 regions of 18-month-old *rol*/+ mice were significantly lower than the other groups.

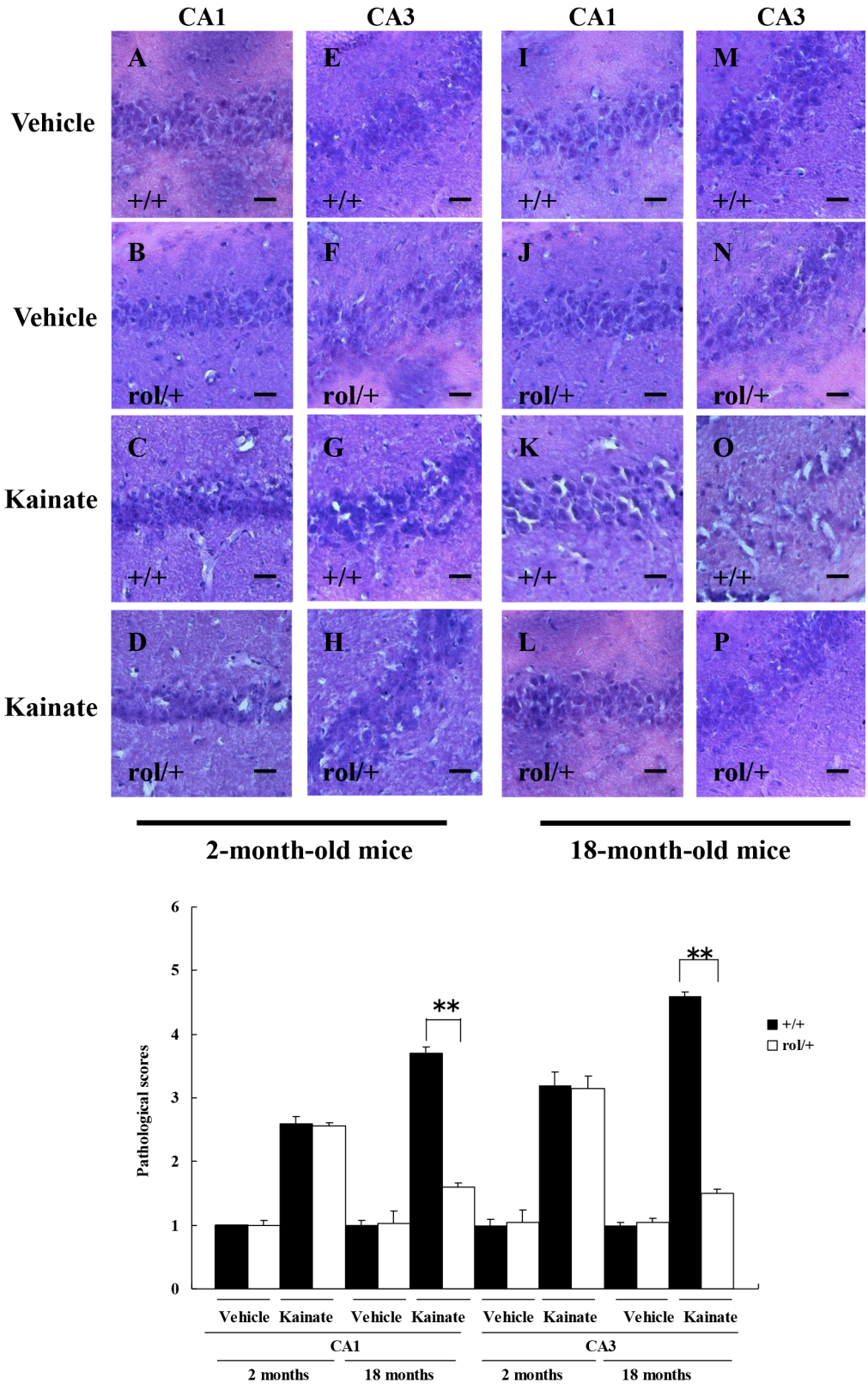
CA1
CA3
CA1
CA3
Vehicle
Vehicle
Kainate
Kainate
A
E
I
M
B
F
J
N
C
G
K
O
D
H
L
P
+/+
rol/+
2-month-old mice
18-month-old mice
Pathological scores
0
1
2
3
4
5
6
**
**
+/+
rol/+
Vehicle
Kainate
Vehicle
Kainate
Vehicle
Kainate
Vehicle
Kainate
CA1
CA3
2 months
18 months
2 months
18 months

Fig. 5. Histopathological findings of neuronal damage induced by kainate. Each section was stained with H&E. After kainate administration in 2-month-old mice, histological features of neuronal damage with pyknotic nuclei, shrinkage, and spongy degeneration were observed in the CA1 (C) and CA3 (G) hippocampal regions of +/+ mice and in the CA1 (D) and CA3 (H) hippocampal regions of *rol*/+ mice. Those pathological indexes in the CA1 (L) and the CA3 (P) regions were apparently reduced in 18-month-old *rol*/+ mice compared to the CA1 (K) and the CA3 (O) regions in 18-month-old +/+ mice. There was no difference between vehicle-treated 2-month-old +/+ (A, E) and *rol*/+ (B, F) mice. There was also no difference between vehicle-treated 18-month-old +/+ (I, M) and *rol*/+ (J, N) mice. Similar results were confirmed in four independent experiments. The average scores of histopathological changes in the CA1 or CA3 regions of the hippocampus after kainate treatment are presented (bottom). The score of each group is expressed as the ratio of score to vehicle-injected 2-month-old +/+ mice. Each bar represents 100 μm. ** $P < 0.01$, compared to the appropriate control (Dunnett's test).

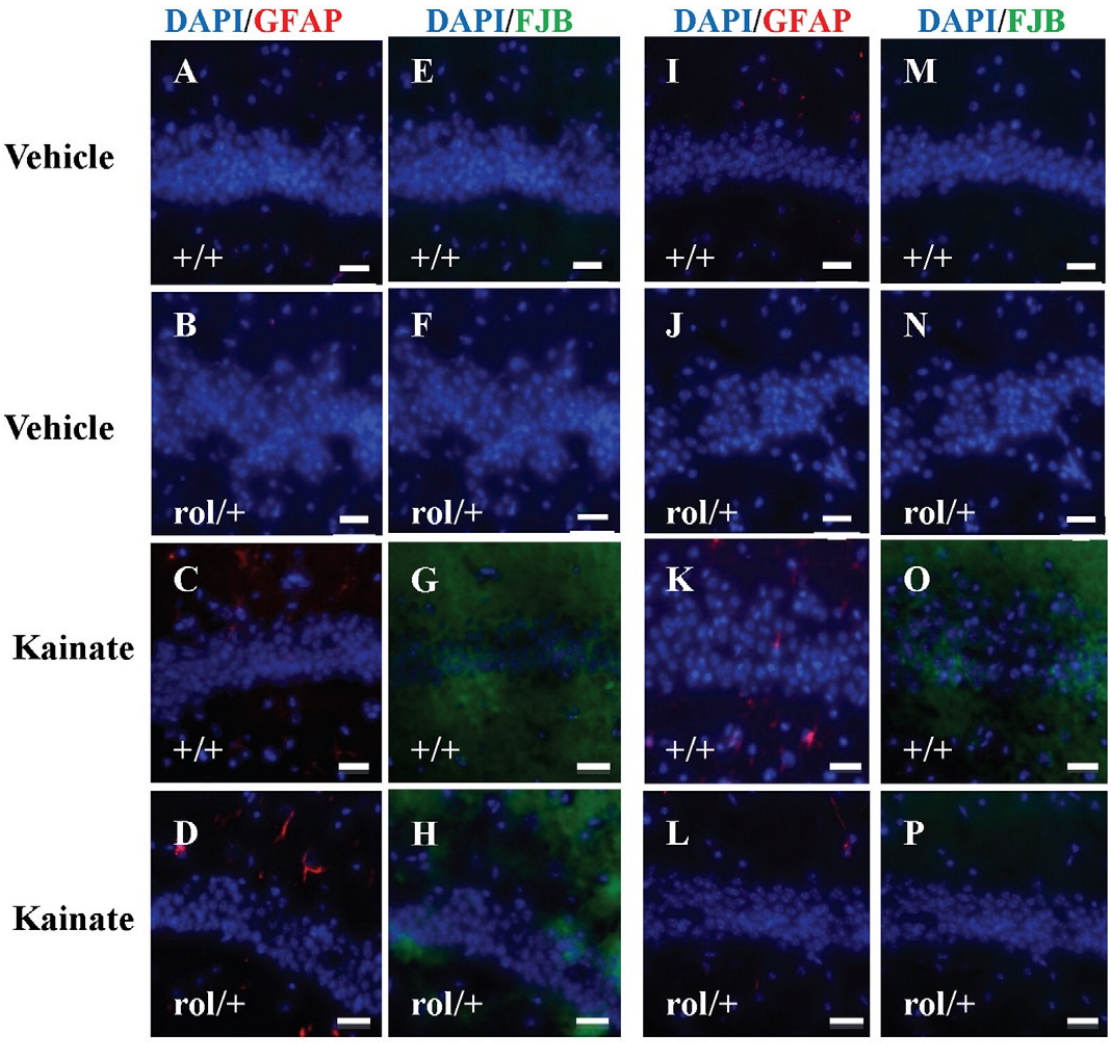
DAPI/GFAP
DAPI/FJB
DAPI/GFAP
DAPI/FJB
Vehicle
Vehicle
Kainate
Kainate
A
E
I
M
B
F
J
N
C
G
K
O
D
H
L
P
+/+
rol/+
2-month-old mice
18-month-old mice

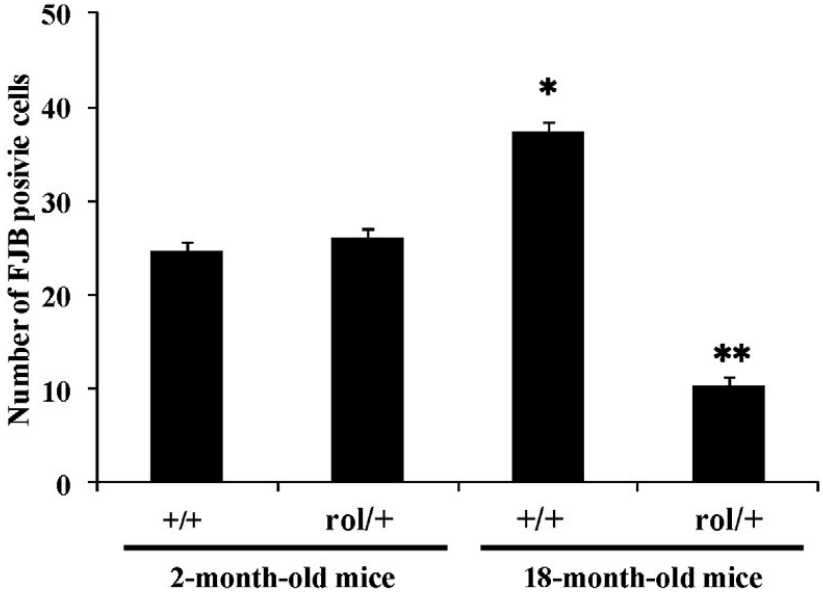
Number of FJB posivie cells
50
40
30
20
10
0
*
**
+/+
rol/+
+/+
rol/+
2-month-old mice
18-month-old mice

Fig. 6. Neuronal damage and appearance of reactive astrocytes in hippocampal CA1 regions induced by kainate. In histopathological studies (top), GFAP-positive astrocytes and FJB-positive neuronal cells were found in the CA1 regions of the hippocampus of 2-month-old +/+ (C, G) and *rol*/+ (D, H) mice after administration of kainate. Although GFAP-positive astrocytes and FJB-positive neuronal cells were also found in 18-month-old +/+ (K, O) mice, they were rarely found in the 18-month-old *rol*/+ (L, P) mice. Although there was no difference between vehicle-treated 2-month-old +/+ (A, E) and *rol*/+ (B, F) mice and between vehicle-treated 18-month-old +/+ (M) and *rol*/+ (N) mice, GFAP-positive cells were barely detected in vehicle-injected 18-month-old +/+ (I) mice but not in vehicle-injected 18-month-old *rol*/+ (J) mice. Similar results were confirmed in six independent experiments. The average numbers of FJB positive cells in the CA1 regions of the hippocampus after kainate treatment are presented (bottom). Each bar represents 100 μm. * $P < 0.05$, ** $P < 0.01$, compared to the appropriate control (Dunnett's test).

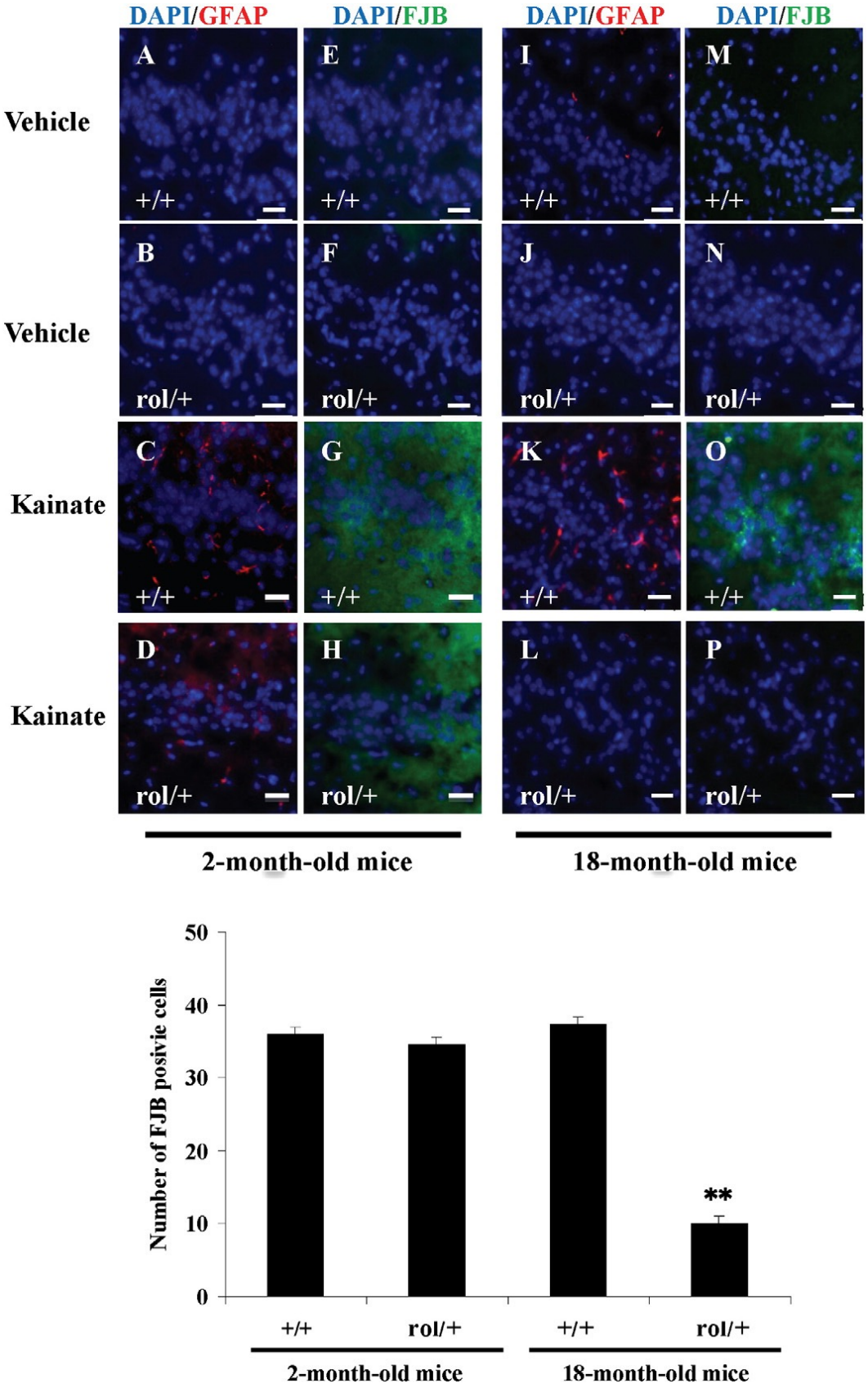
DAPI/GFAP
DAPI/FJB
DAPI/GFAP
DAPI/FJB
Vehicle
Vehicle
Kainate
Kainate
A
E
I
M
B
F
J
N
C
G
K
O
D
H
L
P
+/+
rol/+
2-month-old mice
18-month-old mice
Number of FJB posivie cells
50
40
30
20
10
0
**
+/+
rol/+
+/+
rol/+
2-month-old mice
18-month-old mice

Fig. 7. Neuronal damage and appearance of reactive astrocytes in hippocampal CA3 regions induced by kainate. In histopathological studies (top), GFAP-positive astrocytes and FJB-positive neuronal cells were found in the CA3 regions of the hippocampus of 2-month-old +/+ (C, G) and *rol*/+ (D, H) mice after administration of kainate. Although GFAP-positive astrocytes and FJB-positive neuronal cells were also found in 18-month-old +/+ (K, O) mice, they were rarely found in the 18-month-old *rol*/+ (L, P) mice. Although there was no difference between vehicle-treated 2-month-old +/+ (A, E) and *rol*/+ (B, F) mice and between vehicle-treated 18-month-old +/+ (M) and *rol*/+ (N) mice, GFAP-positive cells were barely detected in vehicle-injected 18-month-old +/+ (I) mice but not in vehicle-injected 18-month-old *rol*/+ (J) mice. Similar results were confirmed in six independent experiments. The average numbers of FJB-positive cells in the CA3 regions of the hippocampus after kainate treatment is shown (bottom). Each bar represents 100 μm. ** $P < 0.01$, compared to the appropriate control (Dunnett's test).

Table 2. Neuronal damage in CA1 after kainate injection.

Mice	GFAP-positive cells		FJB-positive cells	
	Vehicle	Kainate	Vehicle	Kainate
2-month-old +/+	-	++	-	++
2-month-old rol/+	-	++	-	++
18-month-old +/+	+	++	-	+++
18-month-old rol/+	-	+	-	+

Kainate was intraperitoneally injected into mice. Activities were monitored for 1 week after administration of kainate. The results of positively immunostaining cells were rated using the semiquantive scale descrived by Colburn et al. (1997).

Table 3. Neuronal damage in CA3 after kainate injection.

Mice	GFAP-positive cells		FJB-positive cells	
	Vehicle	Kainate	Vehicle	Kainate
2-month-old +/+	-	+++	-	+++
2-month-old rol/+	-	+++	-	+++
18-month-old +/+	+	+++	-	+++
18-month-old rol/+	-	+	-	+

Kainate was intraperitoneally injected into mice. Activities were monitored for 1 week after administration of kainate. The results of positively immunostaining cells were rated using the semiquantive scale descrived by Colburn et al. (1997).

3.4. Low activity of p38 MAPK in the hippocampus of aged *rol*/+ mice after kainate injection

p38 MAPK activity in the hippocampus of 2- and 18-month-old mice was investigated 1 week after injection of vehicle or kainate. Vehicle-injected 2-month-old (*rol*/+, +/+: n = 10 each), vehicle-injected 18-month-old (*rol*/+, +/+: n = 10 each), kainate-injected 2-month-old (*rol*/+, +/+: n = 10 each), and kainate-injected 18-month-old (*rol*/+, +/+: n = 10 each) mice were used. As shown in Fig. 8, levels of pp38 in kainate-injected 18-month-old *rol*/+ mice were markedly low compared to those of kainate-injected age-matched +/+ mice.

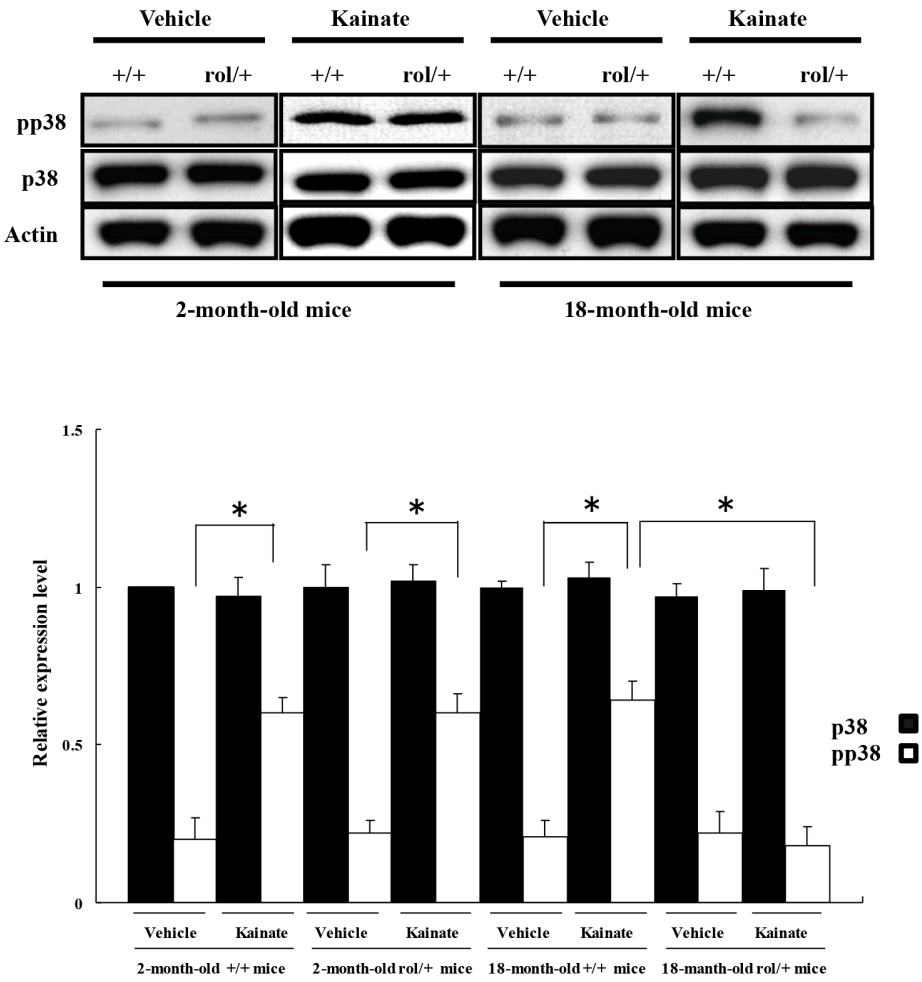

Fig. 8. Phosphorylation of p38 in the hippocampus after injection of kainate. Representative immunoblot (top) and quantification (bottom) of p38 phosphorylated at threonine-180 and tyrosine-182 (pp38), p38, and β-actin (Actin) in 2- and 18-month-old +/+ and *rol*/+ mice 1 week after injection of vehicle or kainate. The amount of each protein was expressed as the ratio of protein to vehicle-injected 2-month-old +/+ mice. * $P < 0.05$, compared to the appropriate control (Dunnett's test).

4. Discussion

This study analyzed the kainate-related seizure and neuronal damage of Cav2.1α_1 mutant strain, *rol*/+ mice. Administration of excessive kainate to mice elicits seizure and causes distinct neuronal degeneration in limbic structures such as the hippocampus (Tikka et al., 2001). As a consequence of the seizures, the mice injected at 20 mg/kg kainate showed neuronal loss, especially in the CA1 and CA3 regions of the hippocampus, followed by activation of glial cells and delayed neural cell death (Namiki et al., 2007). Aged mice are more susceptible to kainate-induced excitotoxicity (Zhang et al., 2008). In the present study, the seizure score and neuronal damages in the hippocampus of 18-month-old +/+ mice administered 20 mg/kg kainate I.P. were also significantly increased compared to those of the 2-month-old +/+ mice, similar to the results from previous report. However, the mechanism is not clear. Interestingly, although no difference was observed between 2-month-old *rol*/+ and +/+ mice injected with 20 mg/kg kainate I.P. in the analyses of seizure and neuronal damage, seizure score and neuronal damage in the CA1 and CA3 regions of the hippocampus of 18-month-old *rol*/+ mice administered 20 mg/kg kainate I.P. were significantly reduced compared to the +/+ mice. A study reported that kainate activates kainate receptors and AMPA receptors (Contractor et al., 2011; Bassani et al., 2013). These results suggest that aged *rol*/+ mice are resistant to kainate-induced excitotoxicity, indicating that the kainate and/or AMPA signal gate may be suppressed, especially in aged *rol*/+ mice. The expression of Grik1, Grik2, Grik3, Grik4, Grik5, Gria1, Gria2, Gria3, and Gria4 was confirmed in the hippocampus using real-time qRT-PCR. However, there was no difference in expression of those kainate receptors and AMPA receptors between *rol*/+ and +/+

mice at age 2 or 18 months. The p38 MAPK pathway is involved in seizure and apoptotic processes (Herlaar and Brown, 1999; Namiki et al., 2007). Hyperactivation of kainate and AMPA receptors has similar effects on p38 signaling (Tsunekawa et al., 2013) and cellular death (Segura Torres et al., 2006).

In a previous study, the p38 MAPK inhibitor SB203580 administration significantly reduced both neuronal loss in the hippocampus and accompanying gliosis (Kim et al., 2004b). These reports indicate that p38 MAPK plays a central role in kainate-induced neuronal damage (Fig. 9). Another study reported that the seizure score of kainate administered heterozygous p38 knockout mouse has significantly decreased than that of +/+ mice (Namiki et al., 2007).

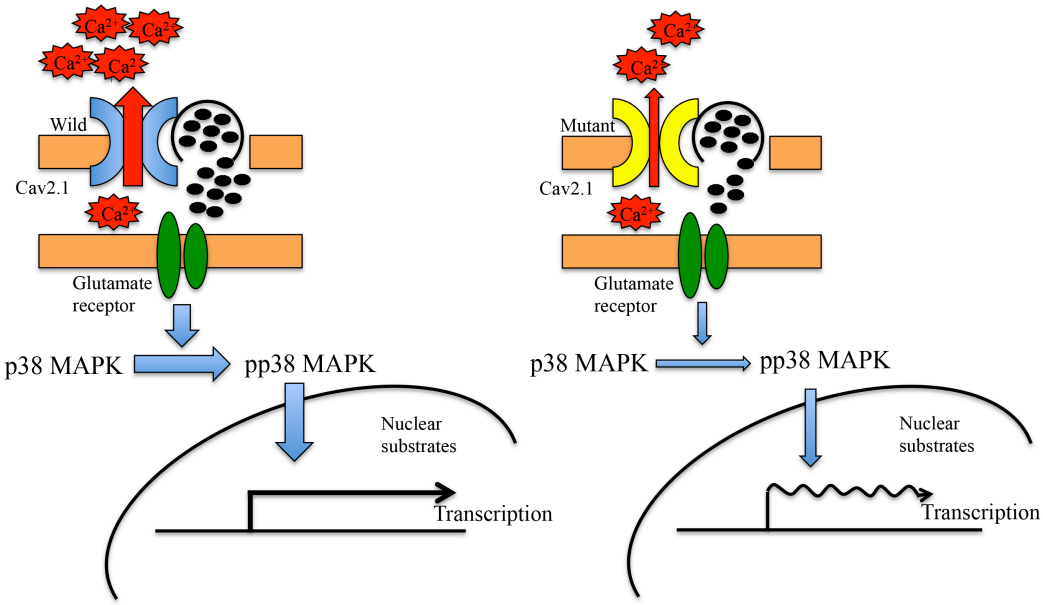

Fig. 9. Putative mechanism for mutant Cav2.1 channel related p38 MAPK signaling. Ca^{2+} concentration plays an important role in neuronal function. Abnormal Cav2.1 channel leads to disturbance of Ca^{2+} influx, resulting in disturbing p38 MAPK signaling.

Aged *rol*/+ mice also exhibited kainate-induced delayed neuronal damage in the CA1 and CA3 regions of the hippocampus. Despite that the roles of each kainate and AMPA receptor were not examined, these results suggest that altering the threshold for glutamate release in depolarization-induced Ca^{2+} influx through the mutant Cav2.1 channel induced abnormal glutamate-related postsynaptic p38 MAPK signaling cascades in aged *rol*/+ mice, leading to lower neuronal loss.

To examine age-related changes in Cav2.1 channel function in the hippocampus, Cav2.1α_1 mRNA patterns using ISH and real-time qRT-PCR analyses were analyzed. *rol*/+ and +/+ mice at the age of 2 or 18 months showed no differences in expression of Cav2.1α_1 mRNA in the hippocampus in ISH studies. In real-time qRT-PCR studies, total-type Cav2.1α_1 mRNA in 18-month-old *rol*/+ mice was expressed at similar levels to that of 2-month-old *rol*/+ mice. However, mutant-type Cav2.1α_1 mRNA increased significantly in 18-month-old *rol*/+ mice compared to 2-month-old *rol*/+ mice. Reportedly, neuronal function is characterized by several neurochemical changes including in peptidergic, cholinergic, monoaminergic, and amino acid neurotransmitters (Dickstein et al., 2007; Foster, 2007; Mora et al., 2007). Although, this study showed that age-associated alternation of the mutated subunit expression pattern was related with the glutamatergic pathway, further studies are warranted to examine the mechanism.

In Western blot analyses, both of the vehicle-treated 18-month-old *rol*/+ mice and 18-month-old +/+ mice showed similar levels of p38 and pp38 expressions. Although the kainate-injected 18-month-old *rol*/+ and +/+ mice also expressed similar levels of p38, expression of pp38 was not increased in 18-month-old *rol*/+ mice in contrast to kainate-injected 18-month-old +/+ mice. These results indicate that although the expression levels of p38 are not influenced by age-related changes in the increased

expression of the mutant-type Cav2.1α_1 gene, the phosphorylation of p38 is affected by the mutant Cav2.1 channel.

The GFAP signal was stronger in vehicle-injected 18-month-old +/+ mice than in vehicle-injected 2-month-old +/+ mice in the CA1 and CA3 regions. This is consistent with a previous report showing that increased GFAP expression is detected in aged animals (Goss et al., 1991). On the other hand, apparent FJB-positive cells undergoing degeneration were not detected in either group. These results indicate that increased GFAP-positive astrocytic responses are due to aging related neuronal survival mechanism.

Recent data from human studies have indicated that the kainate receptor plays a role in depression (Bloss and Hunter, 2010). Genetic ablation of the GluK4 kainate receptor induces anxiolytic and antidepressant-like behavior in mice (Catches et al., 2012). These reports indicate that the kainate receptor can affect emotional behaviors. Other studies regarding p38 MAPK signaling pathway have shown that blockade of the signaling has antidepressive phenotypes (Galeotti and Ghelardini, 2012a, 2012b). Takahashi et al., found reduced anxious and depressive behaviors in 22-month-old *rol*/+ mice but not in 2-month-old *rol*/+ mice (Takahashi et al., 2011). Although a dysfunctional Cav2.1 channel can interfere with various synaptic transmissions, these results suggest that Cav2.1α_1 dysfunction and subsequent p38 MAPK signaling cascades in aged *rol*/+ mice might be responsible, at least partly, for emotional changes. In a previous study, 22-month-old *rol*/+ mice also showed spatial short-term memory deficits based on hippocampus-related object location tests (Takahashi et al., 2009). Expression analysis in hippocampus showed that total Cav2.1α_1 mRNA, including wild-type and mutant-type Cav2.1α_1 mRNA, in 2-month-old *rol*/+ mice was expressed at a level similar to that in 22-month-old *rol*/+ mice. However, wild-type

Cav2.1α_1 mRNA was expressed at a lower level in 22-month-old mice than in 2-month-old mice, and mutant-type Cav2.1α_1 mRNA was expressed at a higher level in 22-month-old versus 2-month-old mice. Although 22-month-old *rol*/+ mice exhibited deficits in cognitive behaviors due to Cav2.1 channel dysfunction, the present study indicates that dysfunctions of Cav2.1-mediated glutamate receptor signaling already occurred at the age of 18 months at least in the hippocampus. In addition, the age-related changes in sensitivity to glutamate could differ among the types of glutamate receptor signaling in *ro*l/+ mice.

In previous studies, the reduction in the P-type Ca^{2+} current amplitude was greater in *la* (60%) than in *rolling Nagoya* (40%) mice (Lorenzon et al., 1998; Mori et al., 2000). Although ataxia is a common symptom in Cav2.1α_1 mutant mice, its severity differs significantly, from mild deficits in *rolling Nagoya* mice to severe ataxia in *la* mice (Pietrobon, 2005; Takahashi, 2012). Heterozygous *la* mice show age-dependent impairment in spatial learning (Alonso et al., 2003). The locations of mutations in each mice are different (Fletcher et al., 1996; Mori et al., 2000). These results indicate that mice of different ages and Cav2.1α_1 gene allelic variants exhibit considerable variability in their phenotypes and that these analyses should be helpful for delineating the association between Cav2.1 function, synaptic transmission, and the postsynaptic signaling cascade.

Age-related changes in sensitivity to kainate in *rol*/+ mice were, at least in part, due to the presence of mutant Cav2.1 channel transcripts and subsequent changes in p38 MAPK signaling. *rol*/+ mice would be a useful model for delineating the relationship between Cav2.1 function, synaptic transmission, and the postsynaptic signaling cascade.

5. Summary

This study is conducted to determine the protective effect of a Cav2.1 channel in kainate-induced neuronal injury using *rolling Nagoya* mice. Based in the analysis data, the findings were as follows:

1. Aged *rol*/+ mice showed lower wild-type Cav2.1α_1 mRNA expression than in 2-month-old mice. The mutant-type Cav2.1α_1 mRNA was expressed at a higher level in 18-month-old versus 2-month-old *rol*/+ mice. These results indicate that mutant-type Cav2.1α_1 expression is age-dependent in *rol*/+ mice.
2. Seizure and neuronal damage were reduced in aged *rol*/+ mice, suggesting that kainate/AMPA signal gate may be suppressed in Cav2.1 channel disfunction leading to excitotoxicity resistance.
3. Neuronal damage and the number of reactive astrocyte were also decreased in aged *rol*/+ mice in CA1 and CA3 regions but not 2-month-old *rol*/+ either +/+ mice. These results suggest that mutant Cav2.1 channel attenuates reactive astrocyte.
4. Expression of pp38 was not increased in kainate-injected aged rol/+ mice in contrast to kainate-injected aged +/+ mice. These results suggest that altering the threshold for glutamate release in depolarization-induced Ca^{2+} influx through the mutant Cav2.1 channel induced abnormal glutamate receptor function and postsynaptic p38 MARK signaling cascades in aged *rol*/+ mice.

Chapter 2.

Protective effect of a Cav2.1 channel in cryogenic brain injury of *rolling Nagoya* mice

1. Introduction

Traumatic brain injury (TBI) is a serious health problem following falls or motor vehicle- or sports-related accidents regardless of age. Fall is the leading cause of TBI (Faul et al., 2010). Many trials using VGCC inhibitors as therapeutic agent have been held (Gurkoff et al., 2013). Administration of Cav1 channel and Cav2.2 channel antagonists showed positive results against brain injury reduced cell death and showed improved cellular function. Cav1 channel antagonists, verapamil and nimodipine, resulted in improvement of cortical injuries. A synthetic Cav2.2 channel antagonist ziconotide also exerted a neuroprotective effect (Gurkoff et al., 2013). A study reported that Cav2.1α_1 mutant *rolling Nagoya* mice had a protective effect against ischemia. *rol*/*rol* mice showed a smaller infarct area compared to that of +/+ mice in ischemic neuronal injury (Tian at al., 2013). A previous study reported that kainate-induced neuronal death indicating that mutant Cav2.1 has protective effect against glutamate related excitotoxiticy. Kainate-injected *rol*/+ mice exhibited milder seizures and fewer degenerated cells compared to +/+ mice (Kim et al., 2014). These results indicate that the mutant Cav2.1α_1 leads to a protective effect against neuronal damage induced by seizure. However, the role of the Cav2.1 channel in brain injury has not been studied.

ω-agatoxin IVA (ω-aga) is a neurotoxin isolated from the venom of a funnel web spider, *Agelenopsis aperta*. It targets neuronal receptor's ion-channels and presynaptic membrane proteins related in neurotransmitter release. Because of its traits, it has been used as a selective antagonist of Cav2.1 channel (Mintz et al., 1992). As it induces a channel activation shift toward more depolarized potentials, it is a dose-dependent gating modifier (Ogura et al., 1998; Pringos et al., 2011). Since it is highly

selective and works in a dose-dependent manner, it is important for research on Cav2.1 channels (Pringos et al., 2011). However, the therapeutic effect of Cav2.1 channel antagonist administration has not been studied.

Cryogenic injury was induced on the cerebrum cortex of mice (Murakami et al., 1999, Nag, 2002). Mechanical damage by cryogenic injury leads to excitotoxicity, involving astrocytes and neurons (Lozano et al., 2015). Abnormal release of neurotransmitters, including glutamate, induces excitotoxicity, independent from blood brain-barrier integrity (Unterberg et al., 2004).

In the present study, to investigate role of Cav2.1 channel in cryogenic brain injury, cryogenic injury-induced cortical brain damage in *rol*/*rol*, +/+, and ω-aga-pretreated +/+ (ω-aga +/+) mice was examined. Also, the possible therapeutic role of the Cav2.1 channel in brain injury by post-treating +/+ mice with ω-aga (ω-aga-post-treated +/+ mice) was investigated one day after the cryogenic procedure.

2. Materials and methods

2.1. Animals

This research was conducted in accordance with the Declaration of Helsinki and was approved by the Animal Experiments Committee of the RIKEN Brain Science Institute (Approval ID: No. H26-2-204). All animals were cared for and treated humanely in accordance with the Institutional Guidelines for Experiments using Animals. Three-month-old (9- to 12-week old) male *rol/rol* and +/+ mice with a C57BL/6 genetic background were used (Tian et al., 2013). Ten *rol/rol*, ω-aga +/+, +/+, ω-aga-post-treated +/+ and vehicle-treated +/+ mice were used in each experiment. All of the mice were housed in groups of three under environmental conditions of 21 ± 2°C, humidity of 55 ± 10%, lighting of 350 lux (at bench level) and a 12:12 light:dark cycle (light from 8:00 am to 8:00 pm). Animals were housed in microisolation cages (MBS7115RHMV, 19.1 × 29.2 × 12.7 cm, Allentown Inc., NJ, USA) with bedding (TEK-FRESH, Harlan Teklad, WI, USA) and given access to irradiated food (5058 PicoLab Mouse Diet 20; LabDiet, MO, USA) and filtered water *ad libitum*. The health status of animals was monitored twice daily.

2.2. Cryogenic model preparation

Animals were anesthetized with a mixture of medetomidine, midazolam, and butorphanol dissolved in saline (0.3 mg/kg body weight (b.w.) medetomidine, 4.0 mg/kg b.w. midazoram, 5.0 mg/kg b.w. butorphanol, I.P.) (Kirihara et al., 2013). An incision was made along the midline of the scalp to expose the skull. Cortical lesions were produced using a liquid nitrogen-cooled metal rod (tip diameter: 2 mm) (Fig. 10) placed on the left parietal bone (coordinates from the bregma: 1.5 mm posterior, 1.5

mm lateral) for 30 sec. The skin incision was closed with a surgical clip. The mice were sacrificed on day 1 or day 7 after cryogenic injury, similar to a previously published protocol (Shi et al., 2012).

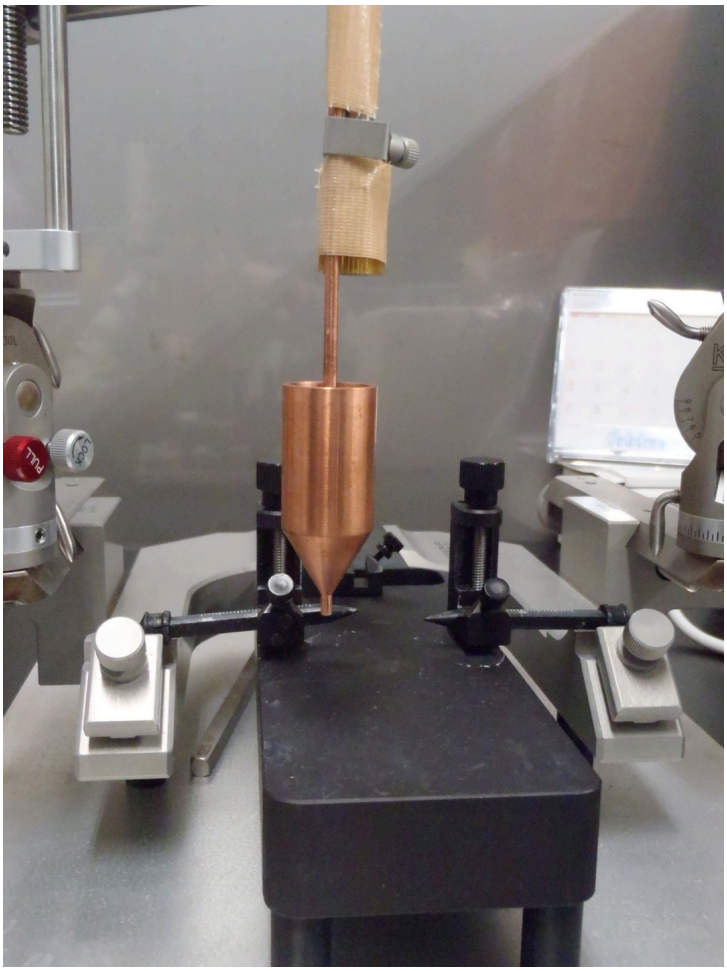

Fig. 10. Stereotaxic equipment and the metal rod (tip diameter 2 mm) used for producing cryogenic TBI model. Cone-shaped copper cylinder is chilled with liquid nitrogen (-196°C) and placed stereotactically on the left parietal skull.

2.3. Determination of lesion size

Lesion size was measured by 2% 2,3,5-triphenyltetrazolium chloride staining (2,3,5-triphenyltetrazolium chloride; Sigma-Aldrich, MO, USA), as described previously (Raslan et al., 2010). The mice were anesthetized with pentobarbital sodium and were intracardially perfused with 0.9% NaCl. The brain was removed and cooled in ice-cold saline for 5 min. The damaged brain area was then dissected into 1 mm thick coronal slices using a brain matrix (Stainless Steel Brain Matrix; Harvard Apparatus, MA, USA). Slices were stained with 2% 2,3,5-triphenyltetrazolium chloride in PBS at 37°C for 30 min and stored in 10% neutral-buffered formalin for visualization. Since the damaged brain is fragile, torn off area was considered as damaged area. Lesion size was measured using ImageJ v1.48 software.

2.4. Drug application

ω-aga (Smartox Biotechnology, Saint-Martin-d'Hères, France) was dissolved in AfCS solution (1× PBS, 0,1% bovine serum albumin). Under anesthesia, 2 μL of 1 ng/μL ω-aga solution or vehicle (AfCS solution) was injected into the lateral ventricle 20 min before the cryogenic injury procedure (coordinates from the bregma: 0.5 mm posterior, 1.0 mm lateral, 2.0 mm ventral) on the other side of the cryogenic injury by craniotomy. The needle was left in place for 2 min following the injection. A group of animals was treated 20 min prior to the cryogenic injury and the other group was treated 24 hr after the injury.

2.5. Immunohistochemistry (IHC)

The IHC protocol used in this study was described previously (Kim et al., 2014). The mice were anesthetized with pentobarbital sodium and were intracardially

perfused with ice-cold 4% PFA in 0.1 M PB (pH 7.4) on day 1 and day 7 after the cryogenic injury procedure. Brains were then removed, placed in fixative for one day followed by 30% sucrose/0.1M PB, and cut coronally into 16 μm thick sections using a cryostat (Microm HM 560; Thermo Scientific, MA, USA). Sections were stained with FJB (Fluoro-Jade® B; Millipore Corporation, MA, USA), anti-GFAP (1:500; Cy3-labeled anti-GFAP, Millipore Corporation) and anti-caspase-9 antibody (1:250; anti-caspase-9 antibody [E23]; Abcam, Cambridge, UK). For pp38 IHC, an anti-pp38 MAP Kinase antibody (1:400; Phospho-p38 MAP kinase (Thr180/Tyr182) antibody; Cell Signaling Technology, MA, USA) was used as the primary antibody with Alexa 488 as the secondary antibody (1:1,000; goat anti-rabbit immunoglobulin [Ig]G antibody; Invitrogen, CA, USA). For double IHC with anti-pp38 and GFAP, and anti-pp38 and NeuN, the same antibodies used above were used for anti-pp38 and GFAP, and anti-NeuN antibody conjugated with Alex 647 (Anti-NeuN antibody [EPR12763]-Neuronal marker (Alexa Fluor® 647); Abcam) was also used. DAPI (DAPI-Fluoromount-G™; Southern Biotech, AL, USA) was used as a nuclear counterstain. Immunostained slides were observed using a conventional fluorescence microscope (IX81, Olympus, Tokyo, Japan) and a digital camera (CoolSNAP™ HQ, Roper Industries, GA, USA) incorporating a charge-coupled device.

2.6. Quantification of neuronal degeneration

GFAP-positive, FJB-positive, caspase-9-positive, and pp38-positive cells were counted in a blind manner. Four square counting frames (641 × 479 μm^2) were placed around the lesion of the four regularly spaced coronal sections from each animal. The numbers of labeled cells in each counting frame around the peri-cryogenic lesion were counted and the average number was used for statistical analysis in all animals.

2.7. Western blot analysis

Experiments were performed according to a previous report (Niimi et al., 2008). The mice were euthanized with an overdose of pentobarbital sodium and decapitated. The injured left cortex was suspended in PRO-PREP™ Protein Extraction Solution (iNtRON Biotechnology, Gyeonggi, Korea). Proteins (20 μg) were electrophoresed on 10% SDS-polyacrylamide gels, and the bands were transferred to polyvinylidene difluoride membranes (Immobilon-P; Millipore Corporation). Commercial antibodies specific for rabbit polyclonal anti-p38 (1:1,000; Abcam) and anti-pp38 MAP Kinase (1:1,000; Phospho-p38 MAP Kinase (Thr180/Tyr182) Antibody; Cell Signaling Technology) were used for immunodetection. Membranes were stripped in stripping buffer, re-probed with p38 antibody, and finally re-probed with mouse monoclonal β-actin antibody (1:5,000; Chemicon, CA, USA), which served as a loading control. Protein signals were visualized and analyzed using Image Studio Digits v5.0 software (LI-COR, NE, USA). Protein bands were boxed, and the integrated intensity of all pixels within the box was calculated against average background levels for a box of the same size. The amount of protein was normalized to that of β-actin.

2.8. Statistical analyses

The data are presented as means ± SEM. Statistical analyses were conducted using Excel Statistics 2006 (SSRI, Tokyo, Japan). The data were analyzed using Dunnett's tests or Mann-Whitney test. The results were considered to be statistically significant at $P < 0.05$ or lower probability of error.

3. Results

3.1. Cryogenic brain injury-induced brain lesion area

Lesion size was assessed on day 1 and day 7 after injury. (*rol/rol*, ω-aga +/+, +/+; n = 10 each). ω-aga toxin or vehicle was injected 20 min prior to the cryogenic injury procedure (Fig. 11A). Significant differences were observed between *rol/rol* and ω-aga +/+, *rol*/*rol* and +/+, and ω-aga +/+ and +/+ mice on day 1 after brain injury (Fig. 11B, top). The lesion was the smallest in *rol/rol* mice, followed by ω-aga +/+ mice. The lesion observed in +/+ mice was the largest. On day 7, there were significant differences between *rol/rol* and +/+, and ω-aga +/+ and +/+ mice (Fig. 11B, bottom). However, no difference was observed between *rol/rol* and ω-aga +/+ mice.

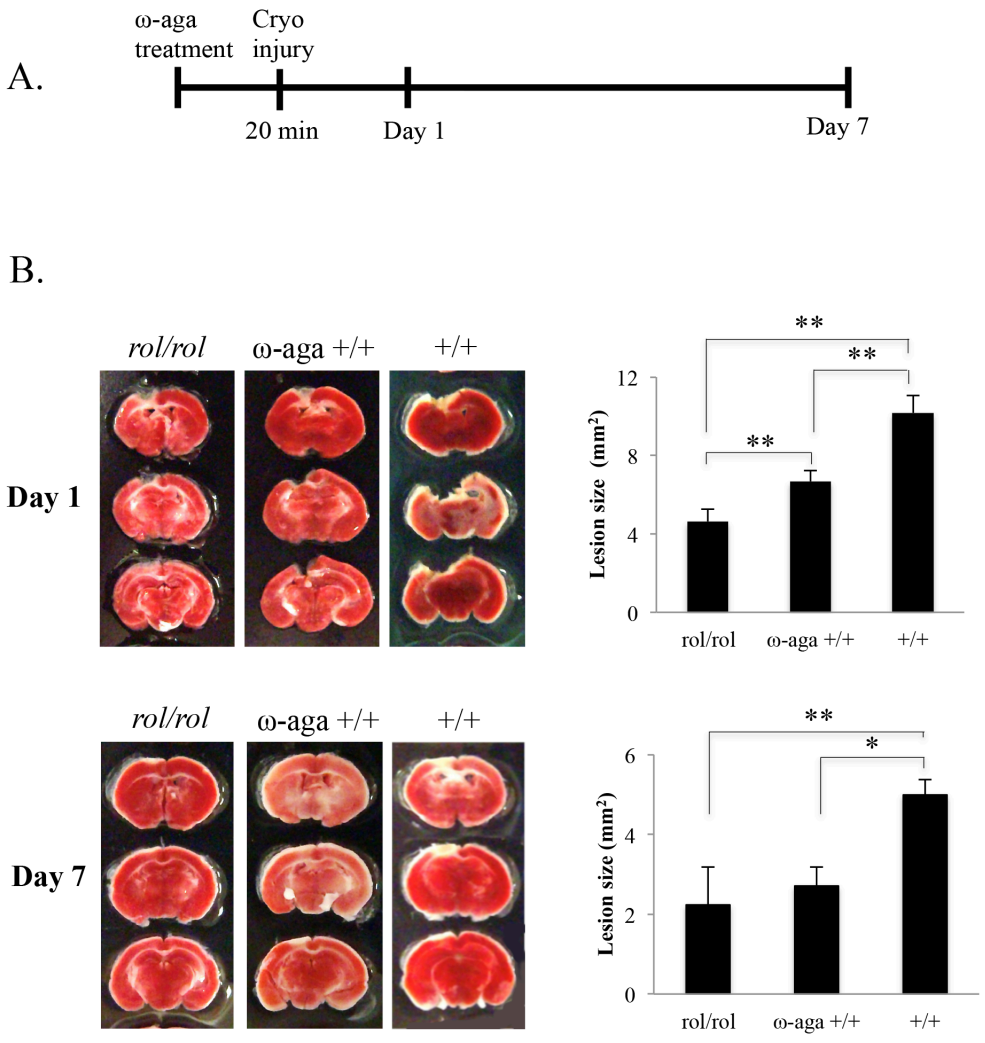

Fig. 11. Lesion area following cryoinjury among each group on day 1 and day 7. ω-aga or vehicle was injected 20 min prior to cryogenic injury. Mice were sacrificed on day 1 and day 7 after cryoinjury (A). Representative photographs of brain slices at on day 1 and day 7 after cryoinjury (B). On day 1, the lesion size was the smallest in *rol/rol* mice followed by ω-aga +/+ mice, then +/+ mice. On day 7, +/+ mice showed the largest lesion size. No significant differences were found between *rol/rol* and ω-aga +/+ mice. * P <0.05, ** P <0.01, compared with the appropriate control (Dunnett's test).

3.2. Astrocyte proliferation following cryogenic brain injury

GFAP has been used as a biomarker for brain injury (Vos et al., 2010) because the anti-GFAP antibody strongly reacts with reactive astrocytes, indicating neurodegeneration. The experimental procedure in this study is shown in Fig. 11A. Immunopositive cells in the lesion periphery were calculated (*rol/rol*, ω-aga +/+, +/+; n = 10 each). On day 1 after injury (Fig. 12, left), the smallest number of reactive astrocytes was observed in *rol/rol* mice, followed by ω-aga +/+ mice. The number of positive cells was the greatest in +/+ mice. On day 7, there were significant differences between *rol/rol* and +/+ and between ω-aga +/+ and +/+ mice. (Fig. 12, right). However, no differences were observed between *rol/rol* and ω-aga +/+ mice.

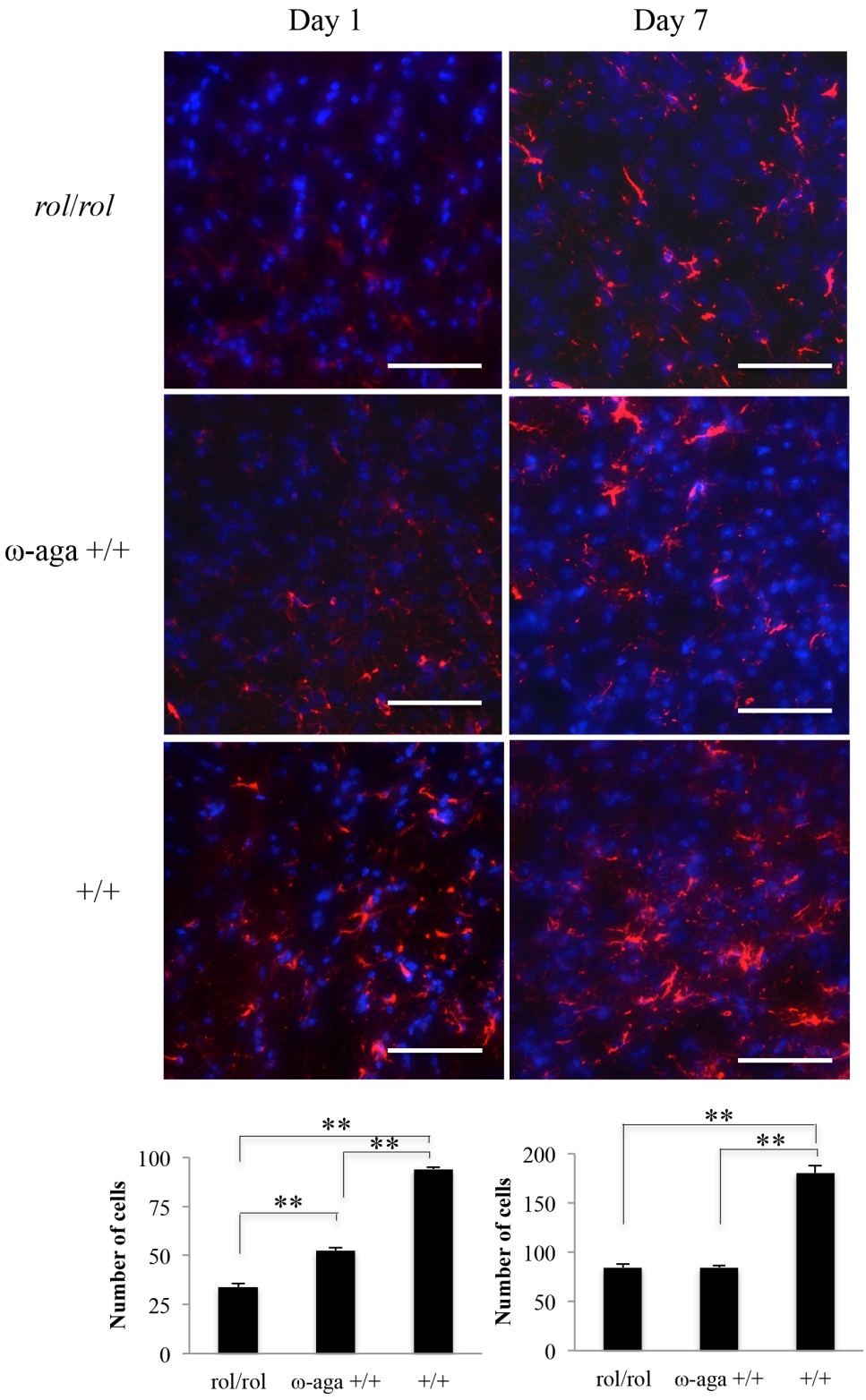
Day 1
Day 7
rol/rol
ω-aga +/+
+/+
Number of cells
100
75
50
25
0
**
**
**
rol/rol
ω-aga +/+
+/+
Number of cells
200
150
100
50
0
**
**
rol/rol
ω-aga +/+
+/+

Fig. 12. Reactive astrocytes following cryoinjury among each group on day 1 and day 7. GFAP signals were found in the lesion periphery on day 1 and day 7 after injury. The smallest number of reactive astrocytes was observed in *rol/rol* mice, followed by ω-aga +/+ mice. The number of positive cells was the greatest in +/+ mice. On day 7, there were significant differences between *rol/rol* and +/+ and between ω-aga +/+ and +/+ mice. Representative sections and the average number of GFAP-positive cells in the lesion periphery are shown. Similar results were confirmed in six independent experiments. Each bar represents 100 μm. ** P <0.01, compared with the appropriate control (Dunnett's test).

3.3. Reduction in neuronal damage following cryogenic brain injury

The number of FJB-positive cells in the lesion periphery was calculated (*rol/rol*, ω-aga +/+, +/+; n = 10 each). The experimental procedure is shown in Fig. 11A. On day 1 after injury (Fig. 13, left), the smallest number of FJB-positive cells was observed in *rol/rol* mice, followed by ω-aga +/+ mice. The greatest number of FJB-positive cells was observed in +/+ mice. On day 7 (Fig. 13, right), there were significant differences between *rol/rol* and +/+ and between ω-aga +/+ and +/+ mice. However, the number of FJB-positive cells did not differ between *rol/rol* and ω-aga +/+ mice. Caspase-9 staining data correlated with that of FJB staining.

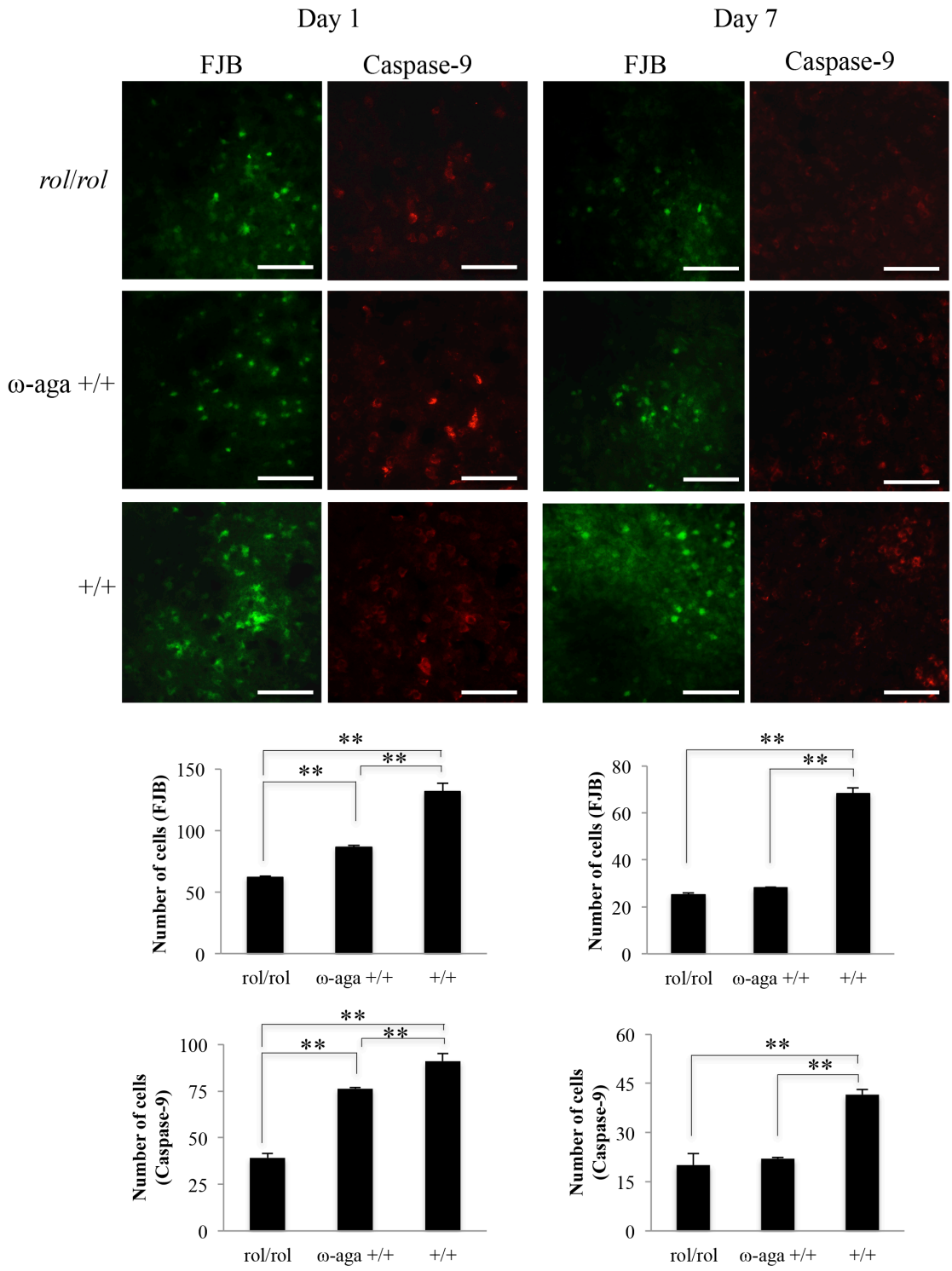
Day 1
Day 7
FJB
Caspase-9
FJB
Caspase-9
rol/rol
ω-aga +/+
+/+
Number of cells (FJB)
150
100
50
0
**
**
**
rol/rol
ω-aga +/+
+/+
Number of cells (FJB)
80
60
40
20
0
**
**
rol/rol
ω-aga +/+
+/+
Number of cells (Caspase-9)
100
75
50
25
0
**
**
**
rol/rol
ω-aga +/+
+/+
Number of cells (Caspase-9)
60
45
30
15
0
**
**
rol/rol
ω-aga +/+
+/+

Fig. 13. Degeneration of neuronal cells following cryoinjury. FJB and caspase-9 signals were found on day 1 and day 7 after injury. The smallest number of FJB positive cells was observed in *rol/rol* mice, followed by ω-aga +/+ mice. The number of positive cells was the greatest in +/+ mice. On day 7, there were significant differences between *rol/rol* and +/+ and, between ω-aga +/+ and +/+ mice. Representative sections, and the average number of FJB-positive and caspase-9-positive cells in the lesion periphery are shown. Similar results were confirmed in six independent experiments. Each bar represents 100 μm. * $P < 0.05$, ** $P < 0.01$, compared with the appropriate control (Dunnett's test).

3.4. Therapeutic effect of ω-aga injection against cryogenic brain injury

ω-aga-post-treated +/+ and vehicle-treated +/+ mice were compared to examine the therapeutic effect of a Cav2.1 antagonist against brain injury, (ω-aga-post-treated +/+, vehicle-treated +/+; n = 10 each). The experimental procedure is shown in Fig. 14A. At 24 hr after cryogenic brain injury, 2 ng of ω-aga or vehicle was injected into the lateral ventricle, and mice were sacrificed on day 7. ω-aga-post-treated +/+ mice had smaller lesions than did vehicle-treated +/+ mice (Fig. 14B). The numbers of GFAP-positive, FJB-positive and caspase-9-positive cells were smaller in ω-aga-post-treated mice than in vehicle-treated +/+ mice (Fig. 15).

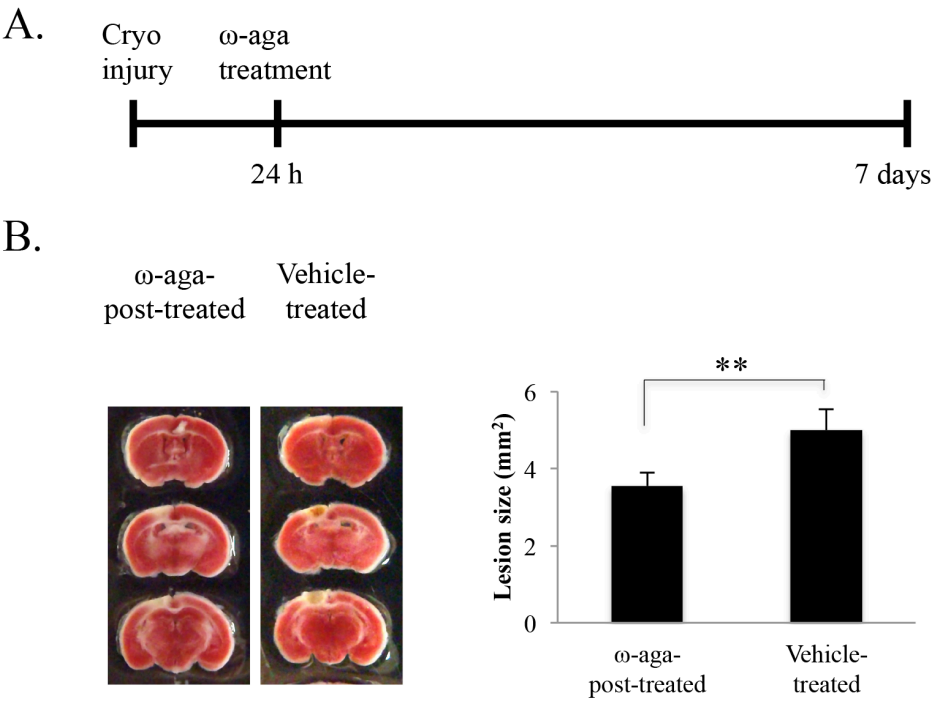

Fig. 14. Therapeutic effect of ω-aga treatment in recovery from cryogenic brain injury. Experimental scheme (A). Lesion areas in ω-aga-post-treated +/+ were smaller than in vehicle-treated +/+ mice (B). ** P <0.01, compared with the appropriate control (Mann-Whitney test).

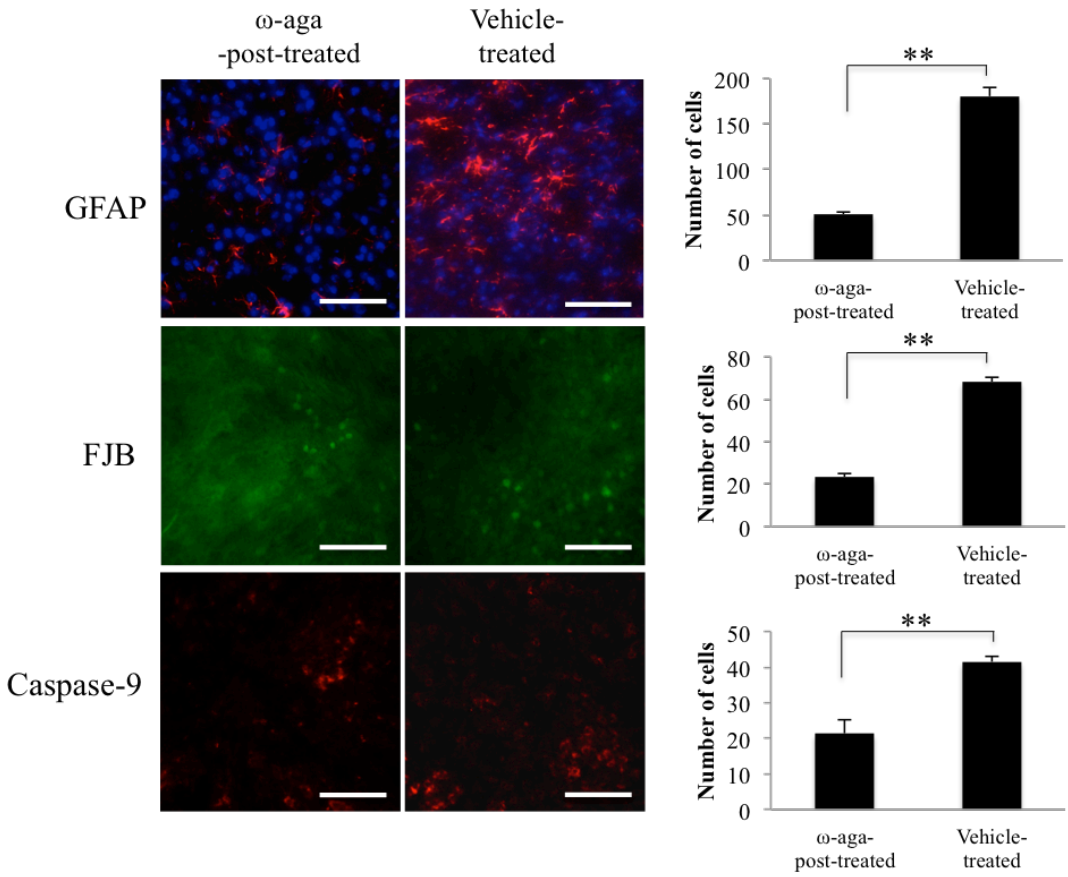

Fig. 15. Representative sections and the average number of GFAP-positive, FJB-positive and caspase-9-positive cells following cryoinjury in ω-aga-post-treated +/+ and vehicle-treated +/+ mice. Similar results were confirmed in six independent experiments. Each bar represents 200 μm. ** P <0.01, compared with the appropriate control (Mann-Whitney test).

3.5. pp38 expression in the ω-aga-treated +/+ mice after cryogenic brain injury

pp38 expression was examined in ω-aga-treated +/+ and vehicle-treated +/+ mice according to the experimental design shown in Fig. 14A (ω-aga-post-treated +/+, vehicle-treated +/+; n = 10 each). pp38 was expressed in neuronal cells but not in astrocytes (Fig. 16). As shown in Fig. 17, the levels of pp38 expression were lower in ω-aga-post-treated +/+ mice than in vehicle-treated +/+ mice.

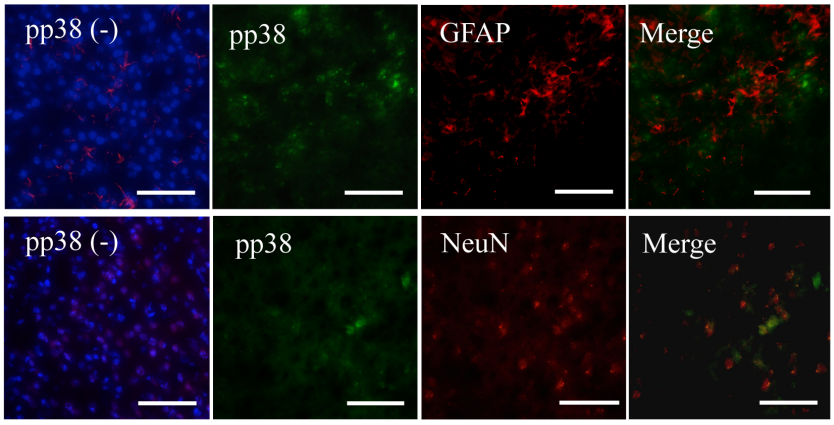

Fig. 16. Fluorescent double immunohistochemical staining of pp38 (green), GFAP (top, red), NeuN (bottom, red) and DAPI (blue) following cryoinjury. The merged pictures of pp38 negative, GFAP and DAPI (top, left), and pp38 negative, NeuN and DAPI (bottom, left) showed no signal of pp38. pp38 and NeuN signals overlap. However, pp38 and GFAP signals are located in different areas. Each bar represents 100 μm.

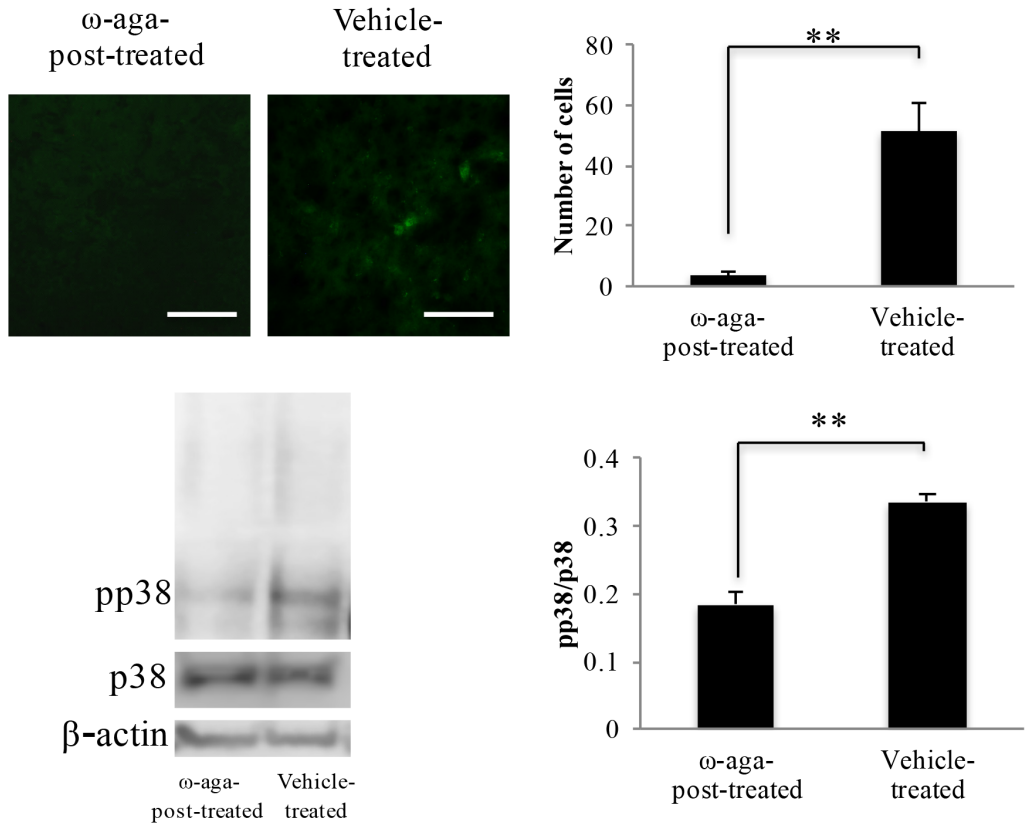

Fig. 17. Effect of a Cav2.1 antagonist on pp38 expression following cryoinjury. A representative section and the average number of pp38-positive (green) cells are shown. The levels of pp38 expression were lower in ω-aga-post-treated +/+ mice than in vehicle-treated +/+ mice. Western blot results correlate with pp38 staining. Similar results were confirmed in six independent experiments. Each bar represents 200 μm. ** P <0.01, compared with the appropriate control (Mann-Whitney test).

4. Discussion

This study using *rol*/*rol* and ω-aga injected mice indicates a protective role of the Cav2.1 channel against cryogenic brain injury. Application of a cryogenic stimulus to the brain resulted in consistent focal destruction of the brain cortex; both dead and surviving cells were observed in the cryolesion core and periphery (Kim et al., 2004a), resembling brain injury in humans.

In previous studies, 2-month-old (5- to 8-week-old) *rol*/+ mice didn't exhibit significant differences in cognition and in behavior compared to wild-type mice (Takahashi et al., 2009; Takahashi et al., 2011), suggesting that normal synaptic functions and neuronal circuit mechanisms in the *rol*/+ mice. Another study reported that 4-month-old (13- to 16-week-old) *rol*/*rol* mice had protective effect against ischemia (Tian et al., 2013). Taken together with these results, to examine the protective effect of Cav2.1 in cryogenic brain injury, we used 12-week-old *rol*/*rol* and wild-type mice in this study.

A study reported that Cav2.1 channels are coupled to glutamate release by using ω-aga administration. Since it binds to presynaptic membrane proteins, it affects glutamate mediated transmission (Turner et al., 1992). The glutamate receptor plays an important role in excitotoxicity-induced damage in brain injury (Gao et al., 2015). The mutant Cav2.1 channel exerted protective effects against ischemic injury (Tian et al., 2013) and kainate-induced seizure and cell damage via suppression of glutamate receptor signaling (Kim et al., 2014). Many studies support that brain injury is associated with glutamate release (Rachmany et al., 2013; Shohami and Biegon, 2014). The smaller lesions in *rol/rol* and ω-aga +/+ mice suggest that the mutant Cav2.1 channel protects from brain injury induced excitotoxicity via disturbing

channel-dependent glutamate signaling. Following administration of 2 ng ω-aga, ω-aga +/+ mice displayed an ataxic gait similar to that of *rol*/*rol* mice (data not shown). Administration of 2 ng ω-aga might have blocked the Cav2.1 channel; however, the effects were not as marked as those observed in *rol/rol* mice. Future studies should confirm the presence of dysfunctional glutamate release through the Cav2.1 channel in the brains of *rol/rol* mice subjected to cryogenic injury. Treating ω-aga post-injury showed a positive effect on recovery. Even though there was no significant difference between ω-aga-pretreated and post-treated mice, ω-aga +/+ mice showed smaller lesions on day 7 compared to ω-aga-post-treated mice (data not shown). Since brains were examined 7 days after injury, further studies are needed to explore long-term therapeutic capacity and determine the timing of Cav2.1 antagonist treatment to maximize the positive effect and minimize negative effects.

Glutamate-induced excitotoxicity is reportedly dependent on activation of the p38 MAPK cascade (Yang et al., 2012b; Rivera-Cervantes et al., 2015). Thus, pp38 expression at the injured site was examined. pp38 signaling was observed in neuronal cells but not in astrocytes. A very weak pp38 signal was observed in the lesion periphery of ω-aga-post-treated +/+ mice, whereas vehicle-treated +/+ mice exhibited a strong p38 signal. Consistent with the result of pp38 examination, ω-aga-post-treated +/+ mice had fewer degenerated cells as well as fewer GFAP-positive cells. This confirms a similar result found in a previous study; the phosphorylation of p38 is affected by the mutant Cav2.1 channel in model of kainate-induced neuronal damage (Kim et al., 2014) (Chapter 1, Fig. 9). These results indicate that the Cav2.1 channel is associated with p38 MAPK signaling and plays an important role in the excitotoxicity observed following brain injury.

In addition to excitotoxicity, astrocytes reportedly contribute to brain damage

(Lozano et al., 2015). My results revealed a population of reactive astrocytes in the lesion periphery. This finding is consistent with a previous report demonstrating that inhibition of a dividing subpopulation of reactive astrocytes had a positive effect on the repair process upon early damage (Pekny and Pekna, 2014). Reactive astrocyte localization in damaged areas is considered beneficial, as it generates a glial scar that protects a healthy brain from the neurotoxic environment; however, too many reactive astrocytes can result in deleterious effects (Pekny and Pekna, 2014). Reactive astrocyte activation and gliosis following brain injury can inhibit tissue regeneration and repair and contribute to permanent disability (Shang et al., 2014). Suppressing glial scar formation promotes axonal regeneration without compromising blood brain-barrier recovery (Yoshioka et al., 2010). Although increased GFAP expression should be evident in reactive astrocytes located around the cryogenic stimulus-induced lesions, *rol/rol* and ω-aga +/+ mice had a weaker GFAP-positive signal than did +/+ mice. A previous study demonstrated upregulation of Cav1.3 channels in reactive astrocytes in a rodent model of neuronal damage (Chung et al., 2001). Another study reported that Gabapentin, which decreases neuronal activity by binding to the α_2/δ-1 subunits of VGCCs, blocks spinal microglial activation (Yang et al., 2012a). This study suggests that the mutant Cav2.1 channel may directly or indirectly suppress astrocyte activation, leading to a faster recovery. However, further studies are warranted.

The results from this study provide evidence that the Cav2.1α_1 mutation exerts a protective effect against cryogenic brain injury. Furthermore, administration of a Cav2.1 inhibitor following injury has a therapeutic effect in a model of cryogenic brain injury. Since the injured mice did not show any abnormal behavior, a positive behavioral effect of ω-aga after brain injury could not be determined. The effect of ω-

aga should be studied in animals that have similar behavioral symptoms after severe brain injury. The Cav2.1 channel antagonist may be used as protective and therapeutic agents against brain injury, especially in the early stages, and *rolling Nagoya* mice could serve as a useful model for brain injury research.

5. Summary

This study is conducted to determine the protective effect of a Cav2.1 channel in brain injury using *rolling Nagoya* mice. Based in the analysis data, the findings were as follows:

1. The lesions were smaller in *rol*/*rol* and ω-aga +/+ mice than +/+ mice. This suggests that mutant Cav2.1 channel has protective effect against excitotoxicity, induced by cryogenic brain injury.
2. Neuronal damage and the number of reactive astrocyte were also decreased in *rol*/*rol* and ω-aga +/+ mice. These results suggest that decreased Ca^{2+} influx due to mutant Cav2.1 channel decreases neuronal damage and reactive astrocyte.
3. Administrating ω-aga into lateral ventricle 24 hr after injury had therapeutic effect.
4. Vehicle-treated mice showed greater level of pp38 expression than ω-aga-post-treated mice. These results indicate that Cav2.1 channel is related with p38 MAPK signaling cascade.

Chapter 3.

Characterization of *tottering-6j* mice

1. Introduction

Cav2.1α_1 mutations have been found in mice and humans. The mutant mice include *rkr*, *tg*, *rolling Nagoya*, *tottering-4j*, *tottering-5j*, *wobbly*, and *pogo* mice (Zwingman et al., 2001; Miki et al., 2008; Lee and Jeong, 2009; Sawada et al., 2009; Takahashi, 2012). These mutant mice display similar symptoms in human disorder, such as ataxia and movement disorder (Takahashi, 2012).

Since mutations in Cav2.1α_1 leads to a wide range of symptoms and disorders, various types of Cav2.1α_1 mutant mice are useful to study channel function and pathogenesis (Pietrobon, 2010). Depending on the location of the mutation, mutant mice exhibit different symptoms. *rkr*, *tg* and *tottering-4j* mice exhibit generalized absence-like seizure, while some mice don't, such as *rolling Nagoya*, *wobby*, or *tottering-5j* mice. The seizures of these mice show bilateral spike-and-wave discharges (SWDs) on electroencephalograms (EEGs), with behavioral arrest similar to absence seizures in humans. As the symptoms are different depending on the mutant location, protein expression patterns also differ among the mutant mice. Abnormal expression patterns of calbindin D-28K (Calb1) (Lee and Jeong, 2009; Sawada et al., 2009), calretinin (Calb2) (Cicale et al., 2002; Nahm et al., 2002; Xie et al., 2007), tyrosine hydroxylase (TH) (Fletcher et al., 1996; Xie et al., 2007; Miki et al., 2008; Sawada et al., 2010), zebrin II (ZebrinII) (Fletcher et al., 1996; Sawada et al., 2009; Sawada et al., 2010), ryanodine receptor 1 (Ryr1) (Cicale et al., 2002), ryanodine receptor 2 (Ryr2) (Sawada et al., 2008), and ryanodine receptor 3 (Ryr3) (Cicale et al., 2002) have been found in the cerebelli of mutant mice.

Tottering-6j mice are generated in the Neuroscience Mutagenesis Facility at The Jackson Laboratory (The Jackson Laboratory, MA, USA) by using ethylnitrosourea

administration (Li et al., 2012). It has a recessive mutation due to a C-to-A base substitution in the Cav2.1α_1 gene, which leads to exon 5 skipping and consequent direct splicing of exon 4 to exon 6 (Li et al., 2012). The effect of this mutation would be expected to be severe, as Cav2.1α_1 protein lacks a significant part of the S4-S5 linker, S5, and part of the S5-S6 linker of domain I (Li et al., 2012). Despite the normal cytoarchitecture of the mutant cerebellum, *tottering-6j* mice display motor dysfunctions. In addition, abnormal TH expression was observed in cerebellar Purkinje cells in the adult mutant mice (Li et al., 2012). However, not much has known regarding other protein expressions.

Here, an electrophysiological analysis was conducted and the pharmacological profile of *tottering-6j* mice was defined. Also, qRT-PCR and histological analyses were performed to determine the expression patterns of proteins in *tottering-6j* mice, including Calb1, Calb2, TH, ZebrinII, Ryr1, Ryr2, and Ryr3.

2. Materials and methods

2.1. Animals

This research was conducted in accordance with the Declaration of Helsinki and was approved by the Animal Experiments Committee of the RIKEN Brain Science Institute (Approval ID: No. H26-2-204). All animals were cared for and treated humanely in accordance with the Institutional Guidelines for Experiments using Animals. The Jackson Laboratory provided the *tottering-6j* mouse strain, which was generated against a C57BL/6 and BALB/cByJ mixed genetic background (Li et al., 2012). In the present studies, *tottering-6j* mice were backcrossed with C57BL/6 mice for three generations, producing *tottering-6j* mice with a C57BL/6 genetic background. Male littermates of *tottering-6j* mice and +/+ mice were used. All of the mice were housed in groups of three under environmental conditions of 21 ± 2°C, humidity of 55 ± 10%, lighting of 350 lux (at bench level) and a 12:12 light:dark cycle (light from 8:00 am to 8:00 pm). Animals were housed in microisolation cages (MBS7115RHMV, 19.1 × 29.2 × 12.7 cm, Allentown Inc., NJ, USA) with bedding (TEK-FRESH, Harlan Teklad, WI, USA) and given access to irradiated food (5058 PicoLab Mouse Diet 20; LabDiet, MO, USA) and filtered water *ad libitum*. The health status of animals was monitored twice daily.

2.2. ISH

9-month-old (33- to 36-week-old) mice were anesthetized with pentobarbital sodium and were intracardially perfused with ice-cold 4% PFA in 0.1 M PB (pH 7.4). Paraffin-embedded blocks and sections of mouse brain tissue for ISH were obtained from Genostaff Co. Ltd. (Tokyo, Japan). Each mouse brain was dissected after

perfusion, fixed with tissue fixative (Gonostaff, Tokyo, Japan) and embedded in paraffin according to proprietary procedures in 6 μm sections. The hybridization protocol was conducted as previously reported (Sakuraoka et al., 2012). The probe for a 691 bp cDNA fragment was designed from positions 6068 to 6748 of Cav2.1α_1 subunit cDNA (Accession Number: NM_007578.3) and labeled with a digoxygenin RNA labeling kit (Roche Diagnostics, Mannhein, Germany). Coloring reactions were performed with NBT/BCIP solution (Sigma-Aldrich, MO, USA) overnight and washed with PBS. The sections were counterstained with Kernechtrot stain solution (Mutoh Pure Chemicals, Tokyo, Japan) and mounted with CC/Mount (Diagnostic Biosystems Inc., CA, USA).

2.3. Real-time qRT-PCR analysis

For Cav2.1α_1 qRT-PCR, 9-month-old mice and for other qRT-PCR, 2-month-old mice were used. The mice were euthanized with an overdose of pentobarbital sodium. Total RNA was isolated from the cerebellum of using TRIzol reagent (Invitrogen, CA, USA). To quantify the mRNA levels of the genes of interest, real-time qRT-PCR was performed using an ABI 7700 Sequence Detection System (Applied Biosystems, MA, USA), and primers specific to each gene (Table 4). Each PCR mixture contained 8.5 μL sterile water, 12.5 μL SYBR Green (Applied Biosystems), 2 μL cDNA (500 ng/μL), 1 μL forward primer (10 pM/μL), and 1μL reverse primer (10 pM/μL). PCR was performed with an initial denaturation at 95°C for 30 sec, followed by 40 cycles, each comprising 95°C for 5 sec and 60°C for 30 sec. All samples were analyzed in duplicate, and the threshold cycle (Ct) value, which reflects the amount of PCR product, was calculated. The relative levels of mRNA expression were determined based on the Ct values after normalization to GAPDH, a housekeeping gene. Each

mRNA expression level in *tottering-6j* mice was calculated relative to that of control +/+ mice.

Table 4. Sequences of primers in this study

Gene	Accession noumber		Sequences (5'-3')
Calb1	MN_009788.4	Sense	CCTTTGTGGATCAATATGGACAGA
		Antisense	TCAGTTGCTGGCATCGAAAG
Calb2	MN_007586	Sense	ATGGAAGCGGCTATATTGATGAGA
		Antisense	TCGGCCAAGGACATGACAC
Th	MN_009377	Sense	CCGCACATTTGCCCAGTTC
		Antisense	TGCACCGTAAGCCTTCAGCTC
ZebrinII	S72537	Sense	TGCCTGACGGAGACCATGAC
		Antisense	CACCATATTGGGCTTGAGCAGA
Ryr1	X83932.1	Sense	CATCGCCATGGGAGTCAAGA
		Antisense	CAAGTAGACCACTACGGCCAGGA
Ryr2	MN_023868.2	Sense	GCAAGCCAGACTGCATGACC
		Antisense	AAATCGCAATGCCCAGCTTC
Ryr3	MN_177652.2	Sense	ATGACGATGAGCCGGATATGAAG
		Antisense	ACGCCCACGTACATGTGGAA
GAPDH	MN_008084.2	Sense	TGTGTCCGTCGTGGATCTGA
		Antisense	TTGCTGTTGAAGTCGCAGGAG

2.4. IHC

2-month-old *tottering-6j* and +/+ mice were used. The mice were anesthetized with pentobarbital sodium and were intracardially perfused with ice-cold 4% PFA in 0.1 M PB (pH 7.4). The brains were removed, embedded in paraffin blocks, and sliced into 4 μm-thick mid-horizontal sections. Five mice were included in each group. The sections were deparaffinized with three changes of xylene and two changes of absolute ethanol. Deparaffinized sections were autoclaved for 10 min at 120ºC. The sections were rehydrated and incubated for 30 min in 1% H_2O_2 in methanol. The slides were incubated for 1 hr in a blocking solution (5% skim milk). The following primary antibodies were used: mouse monoclonal anti-Cab1 (anti-Calbindin-D-28K Clone CB-955; 1:500; Sigma-Aldrich); rabbit monoclonal anti-Calb2 (1:100; Spring Bioscience, CA, USA); rabbit monoclonal anti-TH (1:100; Sigma-Aldrich); rabbit polyclonal anti-ZebrinII (1:100; Novus Biologicals, CO, USA); mouse monoclonal anti-Ryr1 (1:100; Novus Biologicals); rabbit polyclonal anti-Ryr2 (1:100; Novus Biologicals); and rabbit polyclonal anti-Ryr3 (1:100; Millipore Corporation, MA, USA). The following secondary antibodies were used: biotin-conjugated antibodies for Calb1 and Ryr3 staining; Histofine Simple Stain Mouse MAX PO (Nichirei Biosciences Inc., Tokyo, Japan) for Calb2, TH, ZebrinII, and Ryr2 staining; and polyclonal goat anti-rabbit immunoglobulins/horseradish peroxidase for Ryr1 staining. All slides were subjected to 3,3'-diaminobenzidine histochemistry after secondary antibody incubation.

2.5. Quantification of Purkinje cells and granular cells

Purkinje cells were counted in defined areas of cerebellum in a blinded manner. Four square counting frames (1 × 1 mm^2) were placed of the four regularly spaced

sections. The number of Purkinje cells and granular cells in each counting frame and the average number were used for statistical analysis in all animals. Five mice were included in each group.

2.6. Cresyl violet and terminal deoxynucleotidyl transferase-mediated dUTP digoxigenin nick-end-labeling (TUNEL) stainings

The mice were anesthetized with pentobarbital sodium and were intracardially perfused with ice-cold 4% PFA in 0.1 M PB (pH 7.4). The brains were removed, embedded in paraffin blocks, and sliced into 4 μm-thick mid-horizontal sections. Five mice were included in each group. The sections were deparaffinized with three changes of xylene and two changes of absolute ethanol. For cresyl violet staining, the slide-mounted brain sections were incubated with cresyl violet (Sigma-Aldrich) for 30 min at 37°C. An ethanol solution was used to differentiate the stain. The sections were then rinsed with distilled water and air-dried fully. TUNEL staining was performed according to the manufacturer's suggested protocol (NeuroTACS^{TM}II In Situ Apoptosis Detection Kit; Trevigen, Inc., MD, USA).

2.7. EEGs and behavioral observations

To obtain EEGs, *tottering-6j* mice 8- to 16-month of age were anesthetized via I.P. injection of 55 mg/kg pentobarbital sodium. A reference screw electrode was implanted in the left side of the skull [Anterior-Posterior (AP) = −1.4 mm/Lateral (L) = 1.75 mm of bregma]. The cortical EEG electrode was implanted in the right side of the skull (AP 1= 2.2 mm/L = 1.4 mm). The hippocampal EEG electrode was inserted into the hippocampal CA1 area through the right skull [AP = −2.0 mm/L = 1.25 mm/ Depth (ventral from the dura mater) = 1.2 mm of bregma]. A miniature plug was

positioned and fixed on the midline of the parietal bone to afford an electrical connection. After recovery, mice were moved to a recording cage (23 × 16 × 23 cm^3) placed in an electrically shielded and sound-attenuated room. The implanted electrode of each mouse was connected to a cable; this carried signal output. The mice were allowed to move freely with access to food and water *ad libitum*. After about 24 hr of habituation, cortical and hippocampal EEGs were continuously recorded, and behavioral changes observed. EEG signals were amplified (AB-610J, NIHON KOHDEN CO., Tokyo, Japan), filtered (bandpass 0.5-1 kHz) and digitally recorded (256 Hz/channel) on a computer running recording software (Vital Recorder, KISSEI COMTEC Co., Ltd, Nagano, Japan). Abnormal EEG waveforms such as SWDs were analyzed using NeuroScore (Data Sciences International, MN, USA). A SWD lasting for >1 sec was considered an absence-like seizure. When the time interval between two SWDs was <1 sec, the discharges were regarded as a single seizure.

2.8. Effects of antiepileptic drugs

The antiepileptic drugs used were 150 mg/kg ethosuximide (ESM; E7138, Sigma-Aldrich), 200 mg/kg valproic acid (VPA; P4543, Sigma-Aldrich), and 60 mg/kg phenytoin (PHT; 166-12082, Wako Pure Chemical Industries, Ltd., Osaka, Japan). These drug doses were as recommended in previous reports (Heller et al., 1983; Tokuda et al., 2007). Each antiepileptic drug was dissolved in 0.5% (w/v) methylcellulose (131-17811, Wako Pure Chemical Industries, Ltd.). *Tottering-6j* mice 9- to 16-month of age were habituated over a 24 hr period, and the drugs or vehicle were then injected I.P.. Hippocampal EEGs were recorded for 20 min prior to drug administration (reference data) and continuously for 0-20 min, 20-40 min, and 60-80 min after administration. The numbers and durations of SWDs were measured in each

20 min period by reference to the EEG traces. Each animal was given a single dose of one drug (only) on each experimental day.

2.9. Statistical analyses

The data are presented as the mean ± SEM. Statistical analyses were conducted using Excel Statistics 2006 (SSRI, Tokyo, Japan). The data were analyzed using Dunnett's test or ANOVA. Bonferroni post hoc comparisons between groups were performed when appropriate. The results were considered to be statistically significant at a $P < 0.05$ or lower probability of error.

3. Results

3.1. mRNA expression in *tottering-6j* mice.

ISH was used to determine the Cav2.1α_1 expression patterns in 9-month-old *tottering-6j* and +/+ mice (*tottering-6j*: n = 5; +/+: n = 6). The expression patterns were very similar (Fig. 18). An antisense probe showed that both strains exhibited widespread expression of the α_1 subunit in the brain, with particularly high-level expression evident in the olfactory bulb, cerebral cortex, caudate putamen, hippocampus, and cerebellar Purkinje cells. The sense probe yielded no signal from any brain. On gross histological examination of the whole brain and cerebellum, the cytoarchitecture of the mutant brain appeared to be normal.

The expression levels of Cav2.1α_1 in the olfactory bulb, cerebral cortex, caudate putamen, hippocampus, cerebellum, and liver of the two strains of mice were examined via real-time qRT-PCR (*tottering-6j*, +/+: n = 10 each). The relative expression levels of total Cav2.1α_1 did not significantly differ between strains in any of the olfactory bulb (+/+ and *tottering-6j*: 1.05 ± 0.03 and 1.04 ± 0.07), cerebral cortex (+/+ and *tottering-6j*: 1.01 ± 0.08 and 1.07 ± 0.02), caudate putamen (+/+ and *tottering-6j*: 1.02 ± 0.06 and 1.01 ± 0.03), hippocampus (+/+ and *tottering-6j*: 1.05 ± 0.05 and 1.02 ± 0.04), or cerebellum (+/+ and *tottering-6j*: 1.06 ± 0.05 and 1.02 ± 0.07). Liver fractions from either strain did not yield detectable PCR products.

The expression patterns of Calb1, Calb2, TH, ZebrinII, Ryr1, Ryr2, and Ryr3 mRNA were also assessed in the cerebellum of 2-month-old mouse using real-time qRT-PCR analysis (n = 5 each) (Fig. 19). The expression of TH, ZebrinII, and Ryr3 mRNA was significantly increased in *tottering-6j* mice compared with that of +/+ mice. Conversely, the transcript levels of Calb2 were significantly decreased in

tottering-6j mice in comparison with +/+ mice. No amplification products were detected in the fractions that did not include cDNA (data not shown).

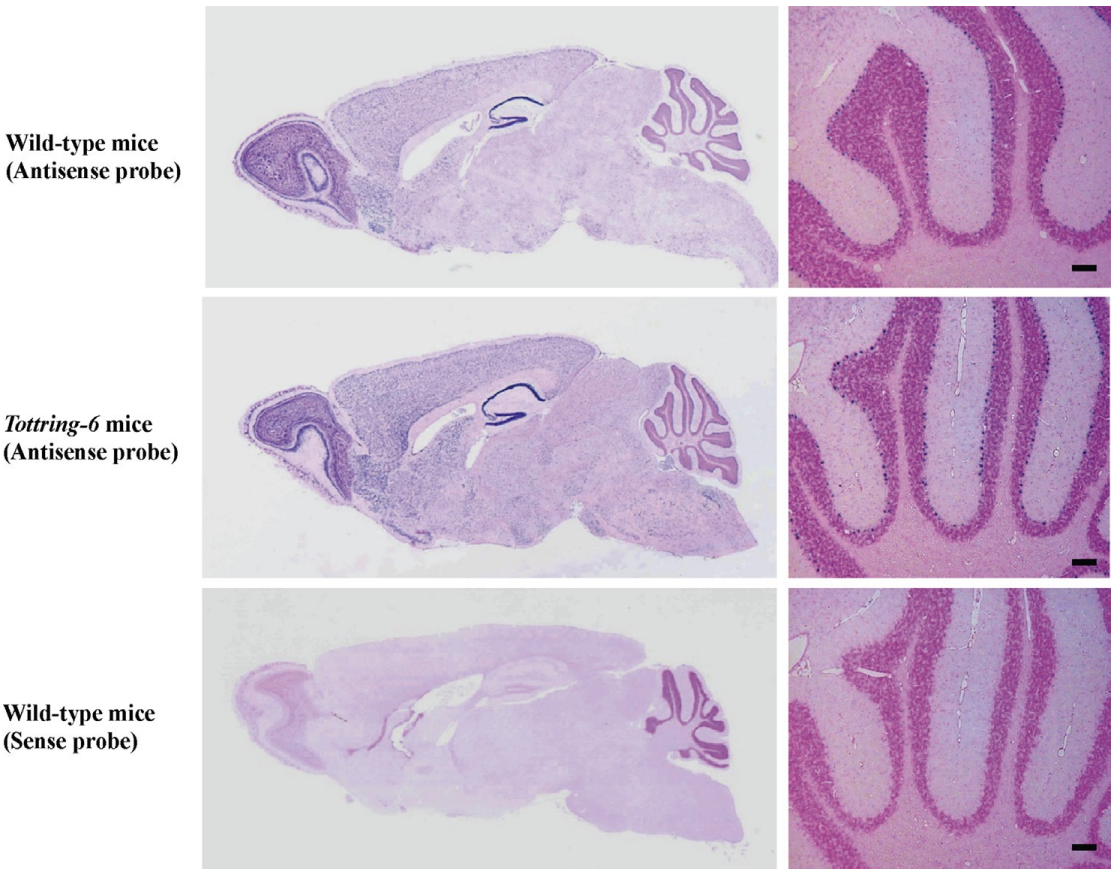

Fig. 18. Expression of Cav2.1α_1 mRNA as revealed by ISH. Representative sagittal sections of the whole brain and large subpopulations of the cerebella of +/+ and *tottering-6j* mice. Each bar represents 200 μm.

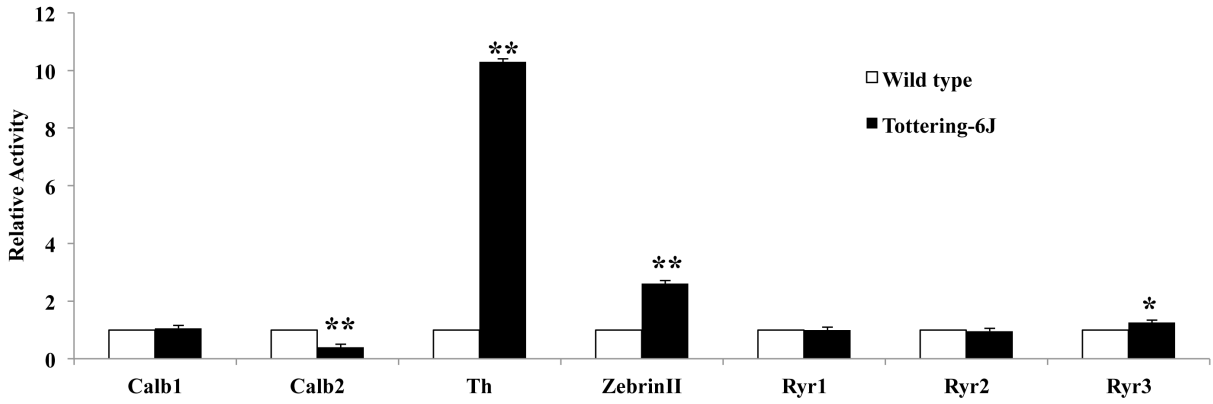

Fig. 19. mRNA expression of Calb1, Calb2, TH, ZebrinII, Ryr1, Ryr2, and Ryr3 genes in the cerebellum of +/+ and *tottering-6j* mice. The data are presented as means ± SEM. * $P < 0.05$, ** $P < 0.01$, compared with the appropriate control (Dunnett's test).

3.2. Histopathological observation of gross morphology and protein expression patterns in the cerebellum of *tottering-6j* mice

Gross morphology and cytoarchitecture were examined by using cresyl violet staining (*tottering-6j*, +/+: n = 5 each). The gross morphology (data not shown) and cytoarchitecture (Fig. 20) of the cerebellum in *tottering-6j* mice were similar to those of +/+ mice. The numbers of Purkinje cells between +/+ and *tottering-6j* mice showed no significant difference (+/+; 37 ± 5 cells/mm^2, *tottering-6*; 41 ± 3 cells/mm^2, $P > 0.05$). The numbers of granule cells between +/+ and *tottering-6j* mice also showed no significant difference (+/+; 2965 ± 35 cells/mm^2, *tottering-6*; 2970 ± 120 cells/mm^2, $P > 0.05$). The expression levels of Calb1, Calb2, TH, ZebrinII, Ryr1, Ryr2, and Ryr3 were determined in the cerebellum of +/+ and *tottering-6j* mice using immunostaining (*tottering-6j*, +/+: n = 5 each). The expression levels of Calb1, Ryr1, and Ryr2 were similar between +/+ and *tottering-6j* mice (data not shown). However, the levels of TH (Fig. 21), ZebrinII (data not shown), and Ryr3 (Fig. 22) were higher than those observed in +/+ mice. Specifically, the expressions of TH and ZebrinII were dramatically increased in the Purkinje cells of *tottering-6j* mice. The Ryr3 expression was increased in the granular layer of *tottering-6j* mice. Despite the abovementioned increased protein expression level in *tottering-6j* mice, the level of Calb2 was lower than that observed in the granular layer of the cerebellum in +/+ mice (Fig. 23).

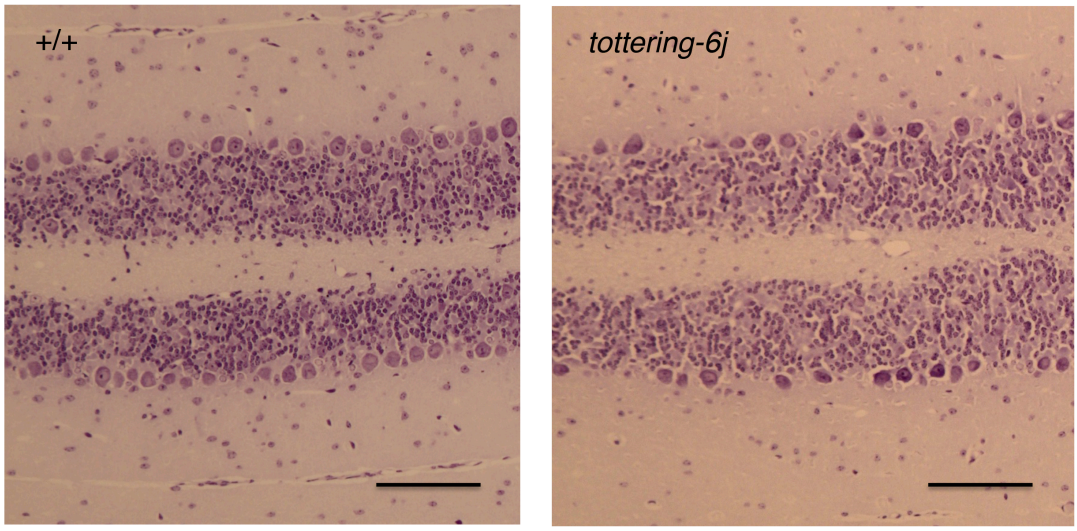

Fig. 20. Cytoarchitecture of the cerebellum. *Tottering-6j* mice had normal cytoarchitecture compared with +/+ mice. There was no Purkinje cell degeneration, and the length of the molecular layer was normal. Each bar represents 200 μm.

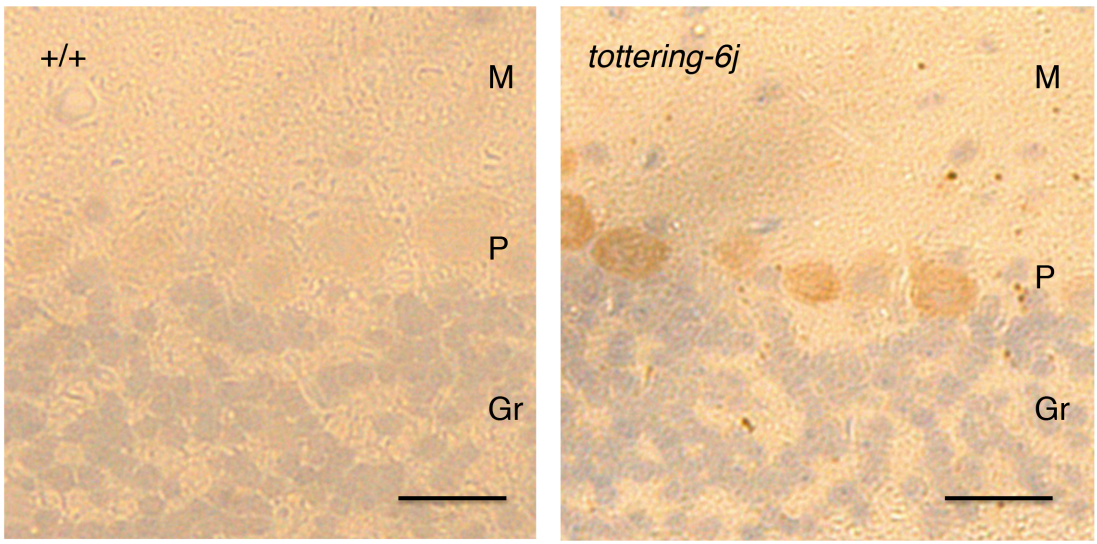

Fig. 21. Expression of TH in the cerebellum. TH expression was increased in the cerebellum of *tottering-6j* mice compared with +/+ mice. Each bar represents 50 μm. M: molecular layer, P: Purkinje cell layer, Gr: granular layer.

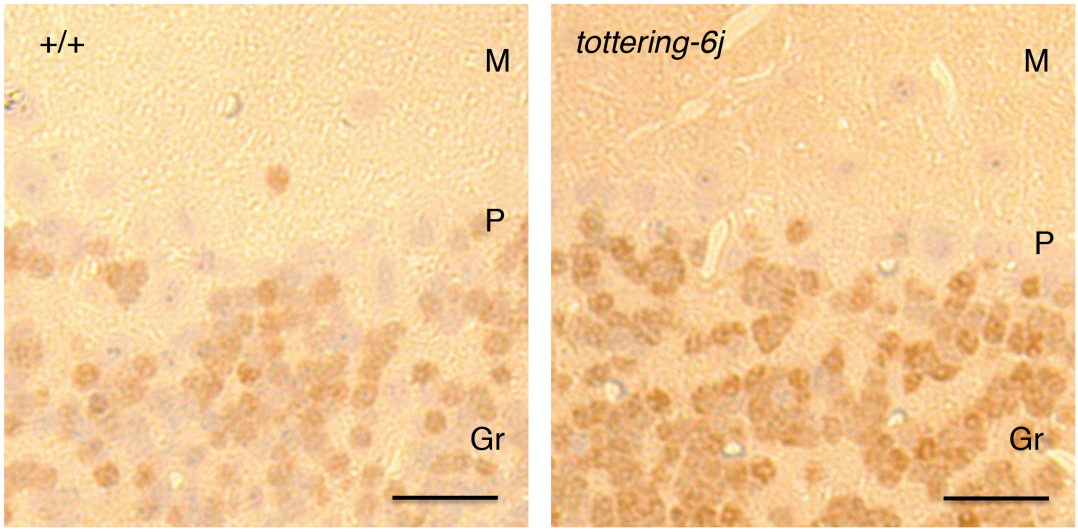

Fig. 22. Expression of Ryr3 in the cerebellum. Ryr3 expression was increased in *tottering-6j* mice compared with +/+ mice. Each bar represents 50 μm. M: molecular layer, P: Purkinje cell layer, Gr: granular layer.

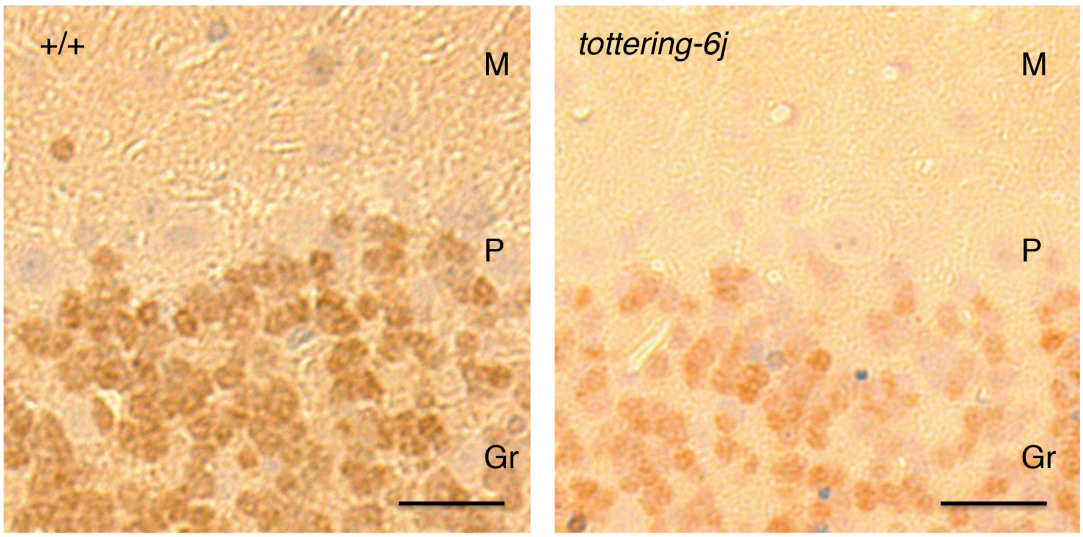

Fig. 23. Expression of Calb2 in the cerebellum. Calb2 expression was decreased in *tottering-6j* mice compared with +/+ mice. Each bar represents 50 μm. M: molecular layer, P: Purkinje cell layer, Gr: granular layer.

3.3. Apoptotic cell death in the cerebellum of *tottering-6j* mice

The amount of apoptosis in the cerebellum of +/+ and *tottering-6j* mice was examined (*tottering-6j*, +/+: n = 5 each). Apoptotic cell death was observed in the granular layer of the cerebellum in *tottering-6j* mice. The number of apoptotic cells was greater in *tottering-6j* mice than in +/+ mice (Fig. 24).

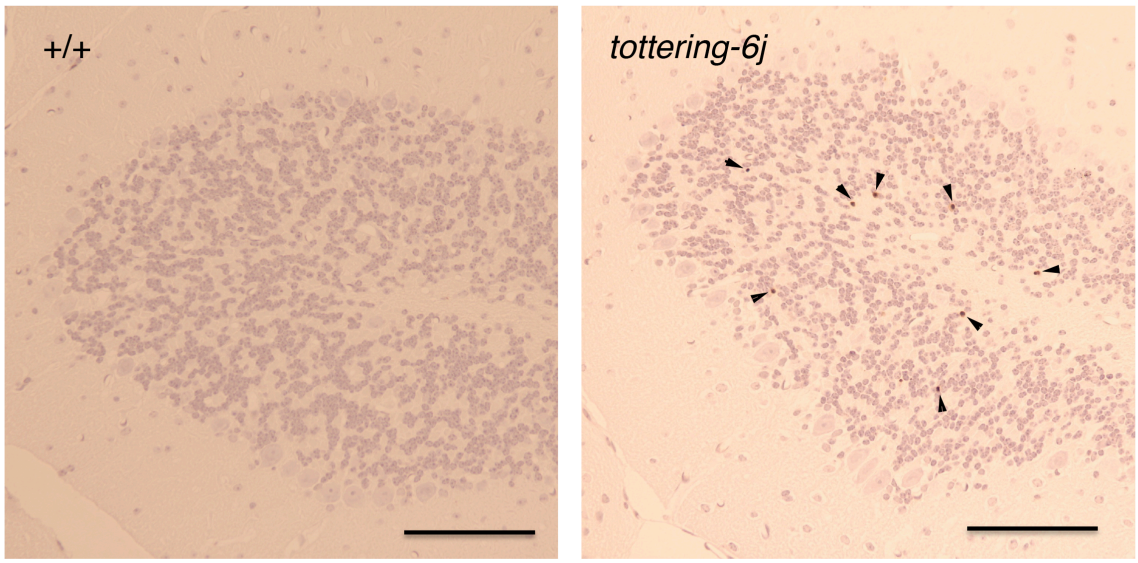

Fig. 24. Apoptotic cell death in the cerebellum. The number of apoptotic cells in *tottering-6j* mice was greater than that of +/+ mice. Apoptotic cells were found in the granular layer. Apoptotic cells are indicated with arrowheads. Each bar represents 200 μm.

3.4. Absence-like seizures of *tottering-6j* mice

To explore whether *tottering-6j* mice exhibited absence-like seizures, EEG and behavioral data were collected. *Tottering-6j* mice exhibited 5-8 Hz SWDs in the bilateral cortex, concomitant with sudden immobility and staring (Fig. 25A). Over 1 hr observation periods of *tottering-6j* mice 9-month of age (n = 5), the mean number of SWDs was 206.80 ± 53.73. The mean duration of each SWD was 2.46 ± 0.13 sec, and the cumulative duration of seizures in the 1 hr was 550.33 ± 139.22 sec. SWDs were also observed in the hippocampus, synchronous with those in the cortex (Fig. 25B).

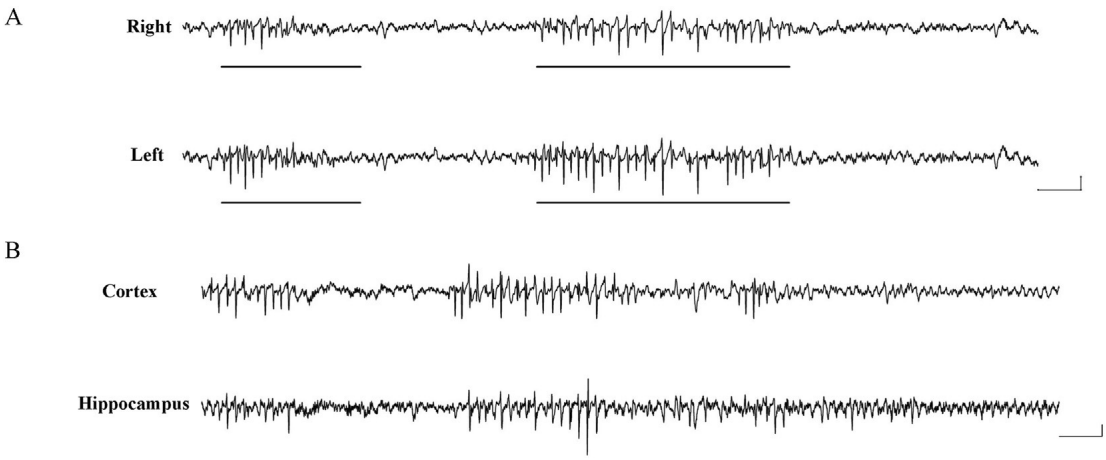

Fig. 25. EEG recordings from *tottering-6j* mice. (A) The right (upper) and left (lower) cortical EEGs exhibited bilateral synchronous 5-8 Hz SWDs concomitant with behavioral arrest (black bar). (B) SWDs occurred synchronously in both the cortex and hippocampus. Calibration: 200 mV and 1 sec.

3.5. Effects of antiepileptic drugs on absence-like seizures in *tottering-6j* mice

The effects of antiepileptic drugs on absence-like seizures in *tottering-6j* mice were examined using the protocol shown in Fig. 26 (n = 8 each). ESM significantly inhibited seizure development 20-40 min after administration and tended to inhibit SWD development 60-80 min after administration. VPA significantly inhibited SWD development at both 20-40 min and 60-80 min after administration. In contrast, PHT did not inhibit SWD development. Vehicle alone did not affect SWD occurrence in *tottering-6j* mice (data not shown).

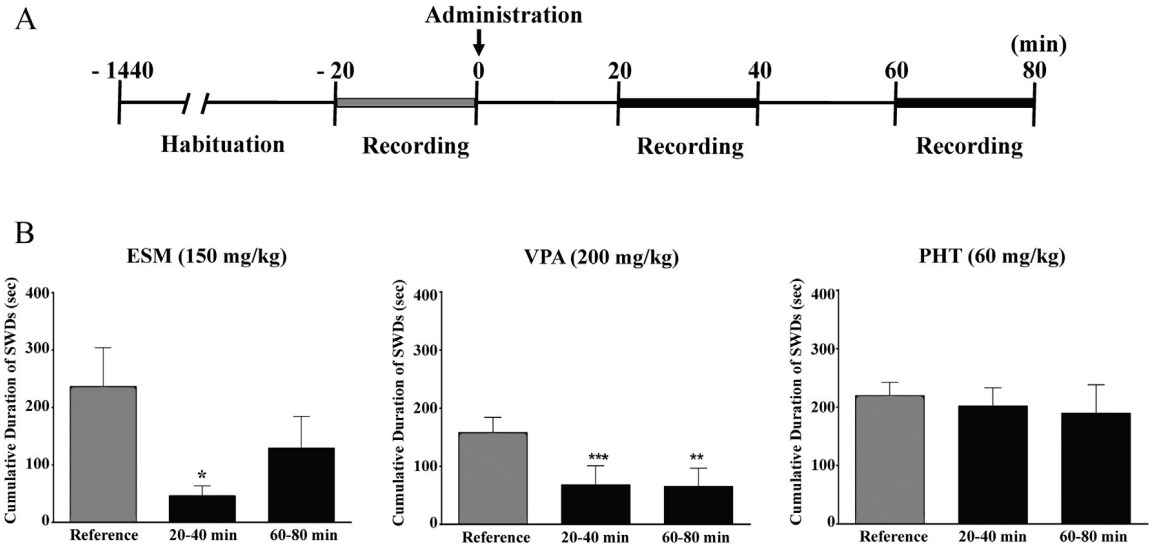

Fig. 26. Effects of antiepileptic drugs on *tottering-6j* mice. (A) The EEG recording schedule. Drugs were administered at 0 min in the experimental period (arrow). (B) Cumulative durations of SWDs in the 20 min intervals before and after drug administration. ESM, VPA, PHT. *$P < 0.05$, ** $P < 0.01$ and *** $P < 0.01$ compared with the reference animals (Bonferroni's multiple comparison test).

4. Discussion

Several animal mutants in the Cav2.1α_1 gene have been reported, and comparison of allelic variants is helpful to clarify the relationships among various structural and physiological abnormalities, protein expression patterns and behavioral deficits. It allows us to understand how the channel functions.

The amino acid sequence in Cav2.1α_1 subunit, the S4-S5 linker, S5, and part of the S5-S6 linker is highly conserved among several vertebral species (Miki et al., 2008). Mutations in Cav2.1α_1 gene have been detected in humans experiencing absence seizures (Gambardella and Labate, 2014), suggesting that it might be involved in epileptogenesis. Absence seizure in humans is a nonconvulsive type of idiopathic generalized epilepsy, exhibiting a brief loss of consciousness (the absence), and SWD evident on EEG during seizure activity (Lüttjohann and Luijtelaar, 2015). Knockout of Cav2.1α_1 gene in mice triggers absence-like seizures in addition to severe ataxia; such animals die 3-4 weeks after birth (Jun et al., 1999), suggesting that the Cav2.1 channel is indispensable.

In the present study, ISH did not reveal any difference in Cav2.1α_1 subunit expression nor in mutant Cav2.1α_1 subunit expression between the brains of +/+ and *tottering-6j* mice. The cerebellum of *tottering-6j* mice showed normal gross morphology, cytoarchitecture while those of some other mice, including *wobbly* and *tg* mice show abnormal morphology. Expression levels of TH, ZebrinII, and Ryr3 were significantly increased in *tottering-6j* mice compared to those of +/+ mice. The Calb2 expression was significantly lower in *tottering-6j* mice than that of +/+ mice. The expression levels of Calb1, Ryr1, and Ryr2 showed no differences between +/+ and *tottering-6j* mice. Data of real time qRT-PCR corresponded with that of IHC.

These results suggest that abnormal Ca^{2+} signaling through the mutation of Cav2.1 in *tottering-6j* strain may affect the transcriptional mechanisms for expression of the Calb2, TH, ZebrinII, and Ryr3 in the cerebellum.

Calb1 and Calb2 are calcium-binding proteins that are abundant in cerebellar cells (Suh et al., 2002; Schwaller, 2014). Calb1 is predominantly expressed in Purkinje cells while Granule cells are the predominant neuron type that expressed Calb2 (Schwaller, 2014). Calb1 expression was decreased in some Cav2.1α_1 mutant strains, including *tg* (Sawada et al., 2009) and *pogo* (Lee and Jeong, 2009) mice, indicating the loss of Purkinje cells. Rhyu et al. reported large axonal swellings and ectopic spines in *rolling Nagoya* mice compared to +/+ mice by using anti-Calb1 staining (Rhyu et al., 1999). High level of Calb1 signal was found in *rolling Nagoya* mice in the study. Based on those findings, Calb1 could be increased in *rolling Nagoya* mice. Further study is warranted. Calb1 expression was normal in *tottering-6j* mice, which supports that *tottering-6j* mice do not exhibit Purkinje cell degeneration.

tg, *wobbly*, and *la* mice exhibited a significant reduction in the expression of Calb2 in the granular layer (Zwingman et al., 2001; Cicale et al., 2002; Nahm et al., 2002). *Tottering-6j* mice also showed low Calb2 expression in the granular cells. However, there was no significant difference between *rolling Nagoya* and +/+ mice (Ando et al., 2005). A previous study reported the absence of Calb2 in the cerebellar granule cells of Calb2 -/- mice, leaded to altered Purkinje cell firing that resulting in impaired motor coordination (Suh et al., 2002). These results indicate that Cav2.1α_1 mutation would lead to signal miscommunication between granular and Purkinje cells and result in ataxia.

TH is an enzyme, which plays an important role in the Cav2.1 related noradrenergic biosynthesis pathway. Correlating to a previous study (Li et al., 2012), persistent TH

expression was found in a specific subset of Purkinje cells in 2-month-old *tottering-6j* mice, which is not expressed in +/+ mice. Cav2.1 mutant mice, including *la* (Fletcher et al., 1996), *tg* (Fletcher et al., 1996), *rolling Nagoya* (Sawada et al., 2010), *tottering-4j* (Miki et al., 2008), *tottering-5j* (Miki et al., 2008), and *wobbly* (Xie et al., 2007) mice also exhibited TH expression. ZebrinII is predominantly expressed in Purkinje cells, however, functional significance is not known (Fletcher et al., 1996). The expression patterns of TH and ZebrinII are similar in *tg*, *la*, and *rolling Nagoya* mice (Fletcher et al., 1996; Sawada et al., 2009; Sawada et al., 2010). ZebrinII is considered as a late-onset pattern marker (Larouche and Hawkes, 2006). Its expression pattern shows array of parasagittal stripes, which is consisted of a few hundred to a few thousand Purkinje cells (Larouche and Hawkes, 2006). A similar pattern was found in *tottering-6j* mice. In addition, the level of the ZebrinII expression was also increased in *tottering-6j* mice.

Ryrs are receptors related in intracellular Ca^{2+} release (Sawada et al., 2008). Three types of Ryrs, including Ryr1, Ryr2 and Ryr3 have been reported and it is known to widely expressed in mouse tissues (Giannini et al., 1995). Ryr1 expression was found in Purkinje cells, however Ryr3 expression was found in granule cells (Giannini et al., 1995; Mori et al., 2000). A study suggested that abnormal Cav2.1 channel might affect Ryr1 and Ryr3 expression through altered Ca^{2+} current in cerebellar neurons (Sawada et al., 2008). Several studies reported altered Ryr expression in Cav2.1 mutant mice. Ryr1 expression was decreased in the cerebellum of *tg* and *rolling Nagoya* mice (Cicale et al., 2002; Sawada et al., 2008). In addition, *rolling Nagoya* mice displayed enhanced Ryr3 expression signal (Sawada et al., 2008). In *tottering-6j* mice, no differences were shown regarding the expression of Ryr1 and Ryr2 compared to that of +/+ mice. The reason for normal Ryr1 expression needs further

study. It is assumed that while *tg* and *rolling Nagoya* type mutation affect Ryr1 expression, *tottering-6j* type mutation does not affect Ryr1 expression.

Apoptosis occurs during cerebellum development. The process completes around postnatal day 17 (Hashimoto and Kano, 2013). TUNEL-positive cells were frequently found in the granule cell layer of *tottering-6j* mice suggesting that cerebellar maturation is also postponed in *tottering-6j* mice, similar to other mutant mice, such as *rolling Nagoya* (Suh et al., 2002) and *la* mice (Fletcher et al., 1996),

This study showed that differences in the location of the Cav2.1α_1 mutation play a significant role in mRNA and protein expression patterns. These altered expression patterns were the results of Ca^{2+} dysregulation resulted by the mutation in the Cav2.1α_1 gene. As mentioned previously, the mutation locations differ in each mutant mouse strain. Table 5 is the example of differences among *rolling Nagoya*, *tottering-6j* and *tg* mice. Therefore, the patterns could be different among the mutant mice. Like those of mutant mice, mutation locations differ in human neurologic disorders, such as FHM1, EA2, and SCA6. Although seven is not enough to be considered as 'profile' to probe human neurologic disorder, this study could be useful in researching about mRNA and protein expressions. Thus, the *tottering-6j* strain is a useful model for cerebellar mRNA and protein expression studies of the Cav2.1 dependent Ca^{2+} signaling.

Table 5. Comparison of *rolling Nagoya*, *tottering-6j* and *tottering* mice

	rolling Nagoya	***tottering-6j***	***tottering***	+/+
Calb1	increased	-	decreased	-
Calb2	-	decreased	decreased	-
TH	increased	increased	increased	-
Ryr1	decreased	-	decreased	-
Ryr2	-	-	N.D.	-
Ryr3	increased	increased	N.D.	-

Reference: Fletcher et al., 1996; Rhyu et al., 1999; Cicale et al., 2002; Ando et al., 2005; Sawada et al., 2008; Sawada et al., 2009; Sawada et al., 2010

EEG recordings and behavioral analyses revealed that *tottering-6j* mice exhibited SWDs concomitant with sudden behavioral arrest, similar to the phenotypes of Cav2.1α_1 subunit mutants, *rkr*, *tg*, and *tottering-4j* mice (Takahashi, 2012), also resembling those of humans. None of *rolling Nagoya*, *wobby*, or *tottering-5j* mice exhibits absence-like seizures (Mori et al., 2000; Xie et al., 2007; Miki et al., 2008). Their mutations are located in the voltage sensor segment (S4) of domain III. The *rkr* and *tg* mutations are located close to the ion-selective pore-forming region of the extracellular segment lying between S5 and S6 of domains III and II, respectively (Fletcher et al., 1996; Zwingman et al., 2001). The mutation in *tottering-4j* mice is located in the S5 region of domain II (Miki et al., 2008). The *tottering-6j* mutation lacks a part of the S4-S5 linker, S5, and part of the S5-S6 linker in domain I (amino acids 213-264) (Li et al., 2012). Such results indicate that the S5 and S5-S6 linker regions play critical roles in preventing absence-like seizures.

In humans, ESM effectively suppresses such seizures, and VPA effectively treats both absence seizures and tonic convulsions. On the other hand, PHT is effective against tonic convulsions but not against absence seizures. ESM and VPA are the first-line antiepileptic drugs recommended in the most commonly used guidelines (Nunes et al., 2012). In *tottering-6j* mice, ESM and VPA also inhibited both the development and duration of SWD, whereas PHT did not, suggesting that the pharmacological profile of the seizures of *tottering-6j* mice is very similar to that of absence seizures in humans. The presence of seizures in this mouse strain supports the association between Cav2.1α_1 mutation and absence seizures.

rkr mice and *tg* mice have similar mutation with *tottering-6j* mice (Li et al., 2012). *rkr* mice have mutation in the S5-S6 linker of domain III. It showed 23% decreased Ca^{2+} current (Kodama et al., 2006). *tg* mice also have mutation in the S5-S6 linker of

domain II. The mutation in *tg* mice resulted in 40% decreased current density (Wakamori et al., 1998). Although tottering-6j mice's mutation is in the S5-S6 linker of domain I (Li et al., 2012), the mutation might result in decreased Ca^{2+} current density.

In conclusion, although further studies are warranted to explain how the *tottering-6j* mutation is related with the structure and function of the Cav2.1 channel in the neuronal network, eventually triggering seizures and altering mRNA expression, *tottering-6j* mouse is also a useful model of human absence epilepsy and Cav2.1 mutation induced neuronal disorder.

5. Summary

This study is conducted to analyze Cav2.1 mutant *tottering-6j* mice. Based on the analysis data, the findings were as follows:

1. ISH and real-time qRT-PCR showed no difference of Cav2.1α_1 expression between *tottering-6j* and +/+ mice.
2. Increased expression of TH, ZebrinII, and Ryr3, and decreased expression of Calb2 were found in the cerebellum of *tottering-6j* mice. These results suggest that decreased Ca^{2+} influx induced by mutant Cav2.1 channel affects transcriptional mechanism of Cab2, TH, ZebrinII and Ryr3 expression in cerebellum.
3. Absence-like seizure in *tottering-6j* mice was inhibited with VPA and ESM, but not PHT. This suggests that the pharmacological characteristic in *tottering-6j* mice resembles to that of human absence seizure.

General Conclusion

VGCCs play important role including neurotransmitter release, neuronal survival, and calcium-dependent gene transcription. Three major presynaptic Cav2 channel, such as Cav2.1, Cav2.2, and Cav2.3 channels, is related in the mechanism of Ca^{2+} dependent excitotoxicity (Takahashi, 2012). While the therapeutic value of Cav2.2 and Cav2.3 channels are known, not much is known about the potential of Cav2.1 channel as a target for therapeutics. Therefore, this study was focused on the Cav2.1 channel.

By using *rolling Nagoya* mice, it was shown that mutant Cav2.1 channel has a protective effect against kainate induced brain injury. The level of pp38 expression was lower in aged *rol*/+ mice than +/+ mice (Chapter 1). Mutant Cav2.1 channel also had a protective effect against cryogenic brain injury. Administrating Cav2.1 inhibitor ω-aga showed positive result in brain damage recovery. pp38 signal was lower in ω-aga post treated mice (Chapter 2).

Glutamate is one of the neurotransmitter coupled to Cav2.1 channel (Turner et al., 1992). Glutamate is a key excitatory neurotransmitter involved in excitotoxicity. Excitotoxicity is a pathological process in neurodegeneration in ischemia or TBI. Excessive level of glutamate over-activates glutamate receptors inducing neuronal death (Connolly and Prehn, 2015). In present study, mutation in Cav2.1 channel had protective effect in kainate-induced seizure and neuronal death, suggesting Cav2.1 channel is coupled to kainate/AMPA receptor signaling. Cav2.1 mutant *rolling Nagoya* mice also showed protective effect against TBI. It is known that glutamate-induced excitotoxicity is dependent on activation of the p38 MAPK cascade (Yang et al., 2012b; Rivera-Cervantes et al., 2015). It is known that p38 MAPK pathway is

involved seizure and apoptotic processes (Herlaar and Brown, 1999; Namiki et al., 2007). Present studies exhibited that low level of pp38 signal in Cav2.1 mutant mice and in ω-aga administered mice. It suggests that altered Ca^{2+} influx by mutant Cav2.1 results in suppression of p38 MAPK signaling.

There are several Cav2.1 mutant mice including *tottering-6j* mice. Each of mutant mice has different traits in neurologic symptoms and gene expression pattern. The absence-seizure of *tottering-6j* mouse resembled that of human. In addition, pharmacological profile was also similar to that of human. Since the mutated location is different from other mutant mice, protein expression patterns also showed differences (Chapter 3). Although further studies are needed to explain the relationships between *tottering-6j* mutation, and the Cav2.1 channel in the neuronal network, resulting having absence-seizures and altering protein expression, *tottering-6j* mouse could be the one for useful model for studying human absence epilepsy, Cav2.1 mutation induced neuronal disorder, and the protein expressions related to these disorders.

Taken together, Cav2.1 channel mutant animals could be useful for studying human Cav2.1 channelopathies, and neuronal functions.

Summary

The voltage-gated Ca^{2+} channel (VGCC) is widely distributed in central nervous system (CNS) and plays important role in Ca^{2+} dependent cell functions. It is a molecular complex consisting of α_1, α_2/δ, β, and γ subunits. Neuronal Cav2.1 channel mediates neuronal functions including post-synaptic signaling cascade, gene transcription and neurotransmitter release, including glutamate. It is an important excitatory neurotransmitter in CNS essential for learning and memory. However, excessive glutamate induces excitotoxicity causing neuronal damage including apoptosis and necrosis. Glutamate binds to specific receptors on post-synapse including, kainate, α-amino-3-hydroxy-5- methyl-4-isoxazolepropionic acid (AMPA), N-methyl-D-aspartate (NMDA) receptors. Kainate administration is used in many studies to induce excitotoxicity model in the brain.

Mutation in human Cav2.1α_1 subunit causes several neurologic disorders, including familiar hemiplegic migraine type 1,episodic ataxia type 2, spinocerebellar ataxia type 6 and epilepsy. The mutations have also discovered in mice including *rolling Nagoya* and *tottering-6j* mice. These mutant mice display neurologic disorders similar to those in human and the symptoms are different among strains.

This study is focused on examining the protective effect of Cav2.1 channel in kainate-induced brain injury and cryogenic brain injury using Cav2.1 mutant *rolling Nagoya*, and absence-like seizures and gene expression in the cerebellum of newly found *tottering-6j* mice.

Rolling Nagoya mouse is a recessive mutant strain, having mutation in voltage-sensing S4 segment located on domain 3 of Cav2.1α_1 subunit, which leads to 40% reduction of Ca^{2+} current amplitude compared to wild-type mice. It exhibits abnormal

movement but not seizures. The mutant Cav2.1α_1 subunit increases with age-dependent manner in heterozygous *rolling Nagoya* (*rol*/+) mice. The sensitivity of kainate-induced seizure had decreased in aged *rol*/+ mice compared to that of wild-type mice. Also neuronal damage and the number of reactive astrocyte in CA1 and CA3 region of hippocampus were also decreased in aged *rol*/+ mice. In addition, western blot result showed that pp38 expression has decreased significantly in aged *rol*/+ mice (Chapter 1). Cryogenic brain damages were induced in 3-month-old homozygous *rolling Nagoya* (*rol*/*rol*) mice. *rol*/*rol* mice showed smaller lesion, less neuronal damage and smaller number of reactive astrocyte in day 1, also in day 7 after the damage. Western blot of Cav2.1 channel inhibitor, ω-agatoxin IVA, -post-treated mice showed lower level of pp38 expression than vehicle-treated mice (Chapter 2). The results of these studies using *rolling Nagoya* mice indicate that Cav2.1 channel is related with p38 MAPK signaling cascade, leading to decreasing neuronal cell death.

The recessive mutant *tottering-6j* mouse lacks a part of the S4-S5 linker, S5, and a part of S5-S6 linker in domain I of the Cav2.1α1 subunit, resulting in poor motor coordination. In this study, homozygous *tottering-6j* mice showed absence-like seizure and pharmacological characteristic similar to those of human. Increased expression of TH, ZebrinII, and Ryr3, and decreased expression of Calb2 were found in the cerebellum of *tottering-6j* mice compared to wild-type mice. These results suggest that Ca^{2+} signaling is related with the seizure and gene expression in cerebellum of *tottering-6j* mice (Chapter 3).

The studies using *rolling Nagoya* mice revealed that Cav2.1 channel has a protective effect in seizure and p38 MAPK signaling related neuronal damage. In addition, the results suggested that Cav2.1 channel inhibitor and pp38 inhibitor could be used as a therapeutic agent against seizure and brain injury. The study using

tottering-6j mice showed that the difference in the location of the Cav2.1α_1 mutation plays a significant role in seizure and gene expression in cerebellum. Thus, *tottering-6j* mice could be useful model for Cav2.1 channel function study.

Acknowledgment

I would like to thank Professor Takashi Kimura, Graduate School of Veterinary Medicine, Hokkaido University, for his encouragement and support this study. I would also like to thank the Director Chitoshi Itakura, RRC, BSI, RIKEN, for the encouragement and support this study. I am very grateful to the Unit Leader Eiki Takahashi, and Dr. Kimie Niimi, Support Unit for Animal Resources Development, RRC, BSI, RIKEN, for the helpful advice and reading this manuscript. I would also like to acknowledge Professor Kazuhiro Kimura and Professor Kenichi Otsuguro, Graduate School of Veterinary Medicine, Hokkaido University, for sitting on my dissertation committee.

References

1. Alonso I, Barros J, Tuna A, Coelho J, Sequeiros J, Silveira I, Coutinho P. Phenotypes of spinocerebellar ataxia type 6 and familial hemiplegic migraine caused by a unique CACNA1A missense mutation in patients from a large family. *Arch Neurol*. 2003;60:610-614.
2. Ando M, Sawada K, Sakata-Haga H, Jeong YG, Takeda N, Fukui Y. Regional difference in corticotropin-releasing factor immunoreactivity in mossy fiber terminals innervating calretinin-immunoreactive unipolar brush cells in vestibulocerebellum of rolling mouse Nagoya. *Brain Res.* 2005;1063:96-101.
3. Asakura K, Matsuo Y, Kanemasa T, Ninomiya M. P/Q-type Ca^{2+} channel blocker omega-agatoxin IVA protects against brain injury after focal ischemia in rats. *Brain Res.* 1997;21:140-145.
4. Bassani S, Folci A, Zapata J, Passafaro M. AMPAR trafficking in synapse maturation and plasticity. *Cell Mol Life Sci*. 2013;70:4411-4430.
5. Bloss EB, Hunter RG. Hippocampal kainate receptors. *Vitam Horm* 2010; 82:167-184.
6. Campiglio M, Flucher BE. The role of auxiliary subunits for the functional diversity of voltage-gated calcium channels. *J Cell Physiol.* 2015;230:2019-2031.
7. Catches JS, Xu J, Contractor A. Genetic ablation of the GluK4 kainate receptor subunit causes anxiolytic and antidepressant-like behavior in mice. *Behav Brain Res.* 2012;228:406-414.
8. Catterall WA. Structure and function of neuronal Ca^{2+} channels and their role in neurotransmitter release. *Cell Calcium.* 1998;24:307-323.

9. Catterall WA. Voltage-gated calcium channels. *Cold Spring Harb Perspect Biol.* 2011;3:a003947.
10. Catterall WA, Few AP. Calcium channel regulation and presynaptic plasticity. *Neuron*. 2008;59:882-901.
11. Catterall WA, Perez-Reyes E, Snutch TP, Striessnig J. International Union of Pharmacology. XLVIII. Nomenclature and structure-function relationships of voltage-gated calcium channels. *Pharmacol Rev*. 2005;57:411-425.
12. Chung YH, Shin CM, Kim MJ, Cha CI. Enhanced expression of L-type Ca^{2+} channels in reactive astrocytes after ischemic injury in rats. *Neurosci Lett.* 2001;302:93-96.
13. Cicale M, Ambesi-Impiombato A, Cimini V, Fiore G, Muscettola G, Abbott LC, de Bartolomeis A. Decreased gene expression of calretinin and ryanodine receptor type 1 in tottering mice. *Brain Res Bull*. 2002;59:53-58.
14. Colburn RW, DeLeo JA, Rickman AJ, Yeager MP, Kwon P, Hickey WF. Dissociation of microglial activation and neuropathic pain behaviors following peripheral nerve injury in the rat. *J Neuroimmunol.* 1997;79:163-175.
15. Connolly NM, Prehn JH. The metabolic response to excitotoxicity - lessons from single-cell imaging. *J Bioenerg Biomembr.* 2015;47:75-88.
16. Contractor A, Mulle C, Swanson GT. Kainate receptors coming of age: milestones of two decades of research. *Trends Neurosci*. 2011;34:154-163.
17. Dickstein DL, Kabaso D, Rocher AB, Luebke JI, Wearne SL, Hof PR. Changes in the structural complexity of the aged brain. *Aging Cell.* 2007;6:275-284
18. Evans RM, Zamponi GW. Presynaptic Ca^{2+} channels--integration centers for neuronal signaling pathways. *Trends Neurosci.* 2006;29:617-624.

19. Faught E. BGG492 (selurampanel), an AMPA/kainate receptor antagonist drug for epilepsy. *Expert Opin Investig Drugs.* 2014;23:107-113.
20. Faul M, Xu L, Wald MM, Coronado VG. Traumatic Brain Injury in the United States: Emergency Department Visits, Hospitalizations and Deaths 2002-2006. Centers for Disease Control and Prevention; Atlanta, GA, USA: 2010.
21. Fletcher CF, Lutz CM, O'Sullivan TN, Shaughnessy JD Jr, Hawkes R, Frankel WN, Copeland NG, Jenkins NA. Absence epilepsy in tottering mutant mice is associated with calcium channel defects. *Cell.* 1996;87:607-617.
22. Foster TC. Calcium homeostasis and modulation of synaptic plasticity in the aged brain. *Aging Cell.* 2007;6:319-325.
23. Fukata Y, Tzingounis AV, Trinidad JC, Fukata M, Burlingame AL, Nicoll RA, Bredt DS. Molecular constituents of neuronal AMPA receptors. *J Cell Biol.* 2005;169:399-404.
24. Galeotti N, Ghelardini C. Regionally selective activation and differential regulation of ERK, JNK and p38 MAP kinase signaling pathway by protein kinase C in mood modulation. *Int J Neuropsychopharmacol.* 2012a;15:781-793.
25. Galeotti N, Ghelardini C. Selective modulation of the PKCε/p38MAP kinase signaling pathway for the antidepressant-like activity of amitriptyline. *Neuropharmacology.* 2012b;62:289-296.
26. Gambardella A, Labate A. The role of calcium channel mutations in human epilepsy. *Prog Brain Res*. 2014;213:87-96.
27. Gao Y, Xu S, Cui Z, Zhang M, Lin Y, Cai L, Wang Z, Luo X, Zheng Y, Wang Y, Luo Q, Jiang J, Neale JH, Zhong C. Mice lacking glutamate

carboxypeptidase II develop normally, but are less susceptible to traumatic brain injury. *J Neurochem*. 2015;134:340-353.

28. Giannini G, Conti A, Mammarella S, Scrobogna M, Sorrentino V. The ryanodine receptor/calcium channel genes are widely and differentially expressed in murine and peripheral tissue. *J Cell Biol*. 1995;128:893-904.
29. Goss JR, Finch CE, Morgan DG. Age-related changes in glial fibrillary acidic protein mRNA in the mouse brain. *Neurobiol Aging.* 1991;12:165-170.
30. Gurkoff G, Shahlaie K, Lyeth B, Berman R. Voltage-gated calcium channel antagonists and traumatic brain injury. *Pharmaceuticals.* 2013;6:788-812.
31. Hashimoto K, Kano M. Synapse elimination in the developing cerebellum. *Cell Mol Life Sci*. 2013;70:4667-4680.
32. Hauser WA, Annegers JF, Kurland LT. Incidence of epilepsy and unprovoked seizures in Rochester, Minnesota: 1935-1984. *Epilepsia.* 1993;34:453-468.
33. Heller AH, Dichter MA, Sidman RL. Anticonvulsant sensitivity of absence seizures in the tottering mutant mouse. *Epilepsia.* 1983;24:25-34.
34. Herlaar E, Brown Z. p38 MAPK signaling cascades in inflammatory disease. *Mol Med Today.* 1999;5:439-447.
35. Heyes S, Pratt WS, Rees E, Dahimene S, Ferron L, Owen MJ, Dolphin AC. Genetic disruption of voltage-gated calcium channels in psychiatric and neurological disorders. *Prog Neurobiol.* 2015;134:36-54
36. Jarvis SE, Zamponi GW. Trafficking and regulation of neuronal voltage-gated calcium channels. *Curr Opin Cell Biol.* 2007;19:474-482.
37. Jun K, Piedras-Rentería ES, Smith SM, Wheeler DB, Lee SB, Lee TG, Chin H, Adams ME, Scheller RH, Tsien RW, Shin HS. Ablation of P/Q-type Ca^{2+} channel currents, altered synaptic transmission, and progressive ataxia in mice

lacking the alpha(1A)-subunit. *Proc Natl Acad Sci USA*. 1999;96:15245-15250.

38. Kim MD, Min DS, Sim KB, Cho H-J, Shin T. Expression and potential role of phospholipase D1 in cryoinjured cerebral cortex of rats. *Histol Histopathol.* 2004a;19:1015-1019.
39. Kim SW, Yu YM, Piao CS, Kim JB, Lee JK. Inhibition of delayed induction of p38 mitogen-activated protein kinase attenuates kainic acid-induced neuronal loss in the hippocampus. *Brain Res.* 2004b;1007:188-191.
40. Kim TY, Yoshimoto T, Aoyama Y, Niimi K, Takahashi E, Itakura C. Age-dependent kainate sensitivity in heterozygous rolling Nagoya Cav2.1 channel mutant mice. *Pharmacol Biochem Behav.* 2014;124:250-259.
41. Kirihara Y, Takachi M, Kurosaki K, Kobayashi Y, Kurosawa T. Anesthetic effect of a mixture of medetomidine, midazolam and butorphanol in two strains of mice. *Exp Anim.* 2013;62:173-180.
42. Kodama T, Itsukaichi-Nishida Y, Fukazawa Y, Wakamori M, Miyata M, Molnar E, Mori Y, Shigemoto R, Imoto K. A Cav2.1 calcium channel mutation rocker reduces the number of postsynaptic AMPA receptors in parallel fiber-Purkinje cell synapses. *Eur J Neurosci.* 2006;24:2993-3007.
43. Larouche M, Hawkes R. From clusters to stripes: the developmental origins of adult cerebellar compartmentation. *Cerebellum.* 2006;5:77-88.
44. Lee CY, Chen CC, Liou HH. Levetiracetam inhibits glutamate transmission through presynaptic P/Q-type calcium channels on the granule cells of the dentate gyrus. *Br J Pharmacol.* 2009;158:1753-1762.
45. Lee NS, Jeong YG. Pogo: a novel spontaneous ataxic mutant mouse. *Cerebellum.* 2009;8:155-162.

46. Leonardi M, Ustun TB. The global burden of epilepsy. *Epilepsia.* 2002;43 Suppl 6:21-25.

47. Li W, Zhou Y, Tian X, Kim TY, Ito N, Watanabe K, Tsuji A, Aoyama Y, Niimi K, Arai T, Takahashi E. New ataxic tottering-6j mouse allele containing a Cacna1a gene mutation. *PLoS ONE.* 2012;7:e44230.

48. Lorenzon NM, Lutz CM, Frankel WN, Beam KG. Altered calcium channel currents in Purkinje cells of the neurological mutant mouse leaner. *J Neurosci.* 1998;18:4482-4489.

49. Lozano D, Gonzales-Portillo GS, Acosta S, de la Pena I, Tajiri N, Kaneko Y, Borlongan CV. Neuroinflammatory responses to traumatic brain injury: etiology, clinical consequences, and therapeutic opportunities. *Neuropsychiatr Dis Treat.* 2015;11:97-106.

50. Lüttjohann A, van Luijtelaar G. Dynamics of networks during absence seizure's on- and offset in rodents and man. *Front Physiol.* 2015;6:16.

51. McCord MC, Lorenzana A, Bloom CS, Chancer ZO, Schauwecker PE. Effect of age on kainate-induced seizure severity and cell death. *Neuroscience.* 2008;154:1143-1153.

52. McKhann GM 2nd, Wenzel HJ, Robbins CA, Sosunov AA, Schwartzkroin PA. Mouse strain differences in kainic acid sensitivity, seizure behavior, mortality, and hippocampal pathology. *Neuroscience.* 2003;122:551-561.

53. Miki T, Zwingman TA, Wakamori M, Lutz CM, Cook SA, Hosford DA, Herrup K, Fletcher CF, Mori Y, Frankel WN, Letts VA. Two novel alleles of tottering with distinct Cav2.1 calcium channel neuropathologies. *Neuroscience.* 2008;155:31-44.

54. Mintz IM, Venema VJ, Swiderek KM, Lee TD, Bean BP, Adams ME. P-type calcium channels blocked by the spider toxin omega-Aga-IVA. *Nature.* 1992;355:827-829.

55. Mora F, Segovia G, del Arco A. Aging, plasticity and environmental enrichment: structural changes and neurotransmitter dynamics in several areas of the brain. *Brain Res Rev.* 2007;55:78-88.

56. Mori Y, Wakamori M, Oda S, Fletcher CF, Sekiguchi N, Mori E, Copeland NG, Jenkins NA, Matsushita K, Matsuyama Z, Imoto K. Reduced voltage sensitivity of activation of P/Q-type Ca^{2+} channels is associated with the ataxic mouse mutation rolling Nagoya (tg(rol)). *J Neurosci.* 2000;20:5654-5662.

57. Murakami K, Kondo T, Yang G, Chen SF, Morita-Fujimura Y, Chan PH. Cold injury in mice: a model to study mechanisms of brain edema and neuronal apoptosis. *Prog Neurobiol.* 1999;57:289-299.

58. Nag S. The blood-brain barrier and cerebral angiogenesis: Lessons from the cold-injury model. *Trends Mol Med.* 2002;8:38-44.

59. Nahm SS, Tomlinson DJ, Abbott LC. Decreased calretinin expression in cerebellar granule cells in the leaner mouse. *J Neurobiol.* 2002;51:313-322.

60. Namiki K, Nakamura A, Furuya M, Mizuhashi S, Matsuo Y, Tokuhara N, Sudo T, Hama H, Kuwaki T, Yano S, Kimura S, Kasuya Y. Involvement of p38alpha in kainate-induced seizure and neuronal cell damage. *J Recept Signal Transduct Res.* 2007;27:99-111.

61. Niimi K, Takahashi E, Itakura C. Improved short-term memory and increased expression of NR2B observed in senescence-accelerated mouse (SAM)P6. *Exp Gerontol.* 2008;43:847-852.

62. Nunes VD, Sawyer L, Neilson J, Sarri G, Cross JH. Diagnosis and management of the epilepsies in adults and children: summary of updated NICE guidance. *BMJ.* 2012;344:e281.

63. Oda S. The observation of rolling mouse Nagoya (*rol*), a new neurological mutant, and its maintenance. *Exp Anim.* 1973;22:281-286.

64. Ogura H, Furuya Y, Teramoto T, Niidome T, Nishizawa Y, Yamanishi Y. Peptide N- and P/Q-type Ca^{2+} blockers inhibit stimulant-induced hyperactivity in mice. *Peptides.* 1998;19:1017-1022.

65. Pekny M, Pekna M. Astrocyte reactivity and reactive astrogliosis: costs and benefits. *Physiol Rev.* 2014;94:1077-1098.

66. Pietrobon D. Function and dysfunction of synaptic calcium channels: insights from mouse models. *Curr Opin Neurobiol.* 2005;15:257-265.

67. Pietrobon D. Cav2.1 channelopathies. *Pflugers Arch.* 2010;460:375-393.

68. Pringos E, Vignes M, Martinez J, Rolland V. Peptide neurotoxins that affect voltage-gated calcium channels: A close-up on ω-agatoxins. *Toxins (Basel).* 2011;3:17-42.

69. Rachmany L, Tweedie D, Rubovitch V, Yu QS, Li Y, Wang JY, Pick CG, Greig NH. Cognitive impairments accompanying rodent mild traumatic brain injury involve p53-dependent neuronal cell death and are ameliorated by the tetrahydrobenzothiazole PFT- α. *PLoS One*. 2013;8:e79837

70. Rajendra W, Armugam A, Jeyaseelan K. Neuroprotection and peptide toxins. *Brain Res Brain Res Rev.* 2004;45:125-141.

71. Raslan F, Schwarz T, Meuth SG, Austinat M, Bader M, Renne T, Roosen K, Stoll G, Sirén AL, Kleinschnitz C. Inhibition of bradykinin receptor B1

protects mice from focal brain injury by reducing blood-brain barrier leakage and inflammation. *J Cereb Blood Flow Metab.* 2010;30:1477-1486.

72. Rhyu IJ, Oda S, Uhm CS, Kim H, Suh YS, Abbott LC. Morphologic investigation of rolling mouse Nagoya (tg(rol)/tg(rol)) cerebellar Purkinje cells: an ataxic mutant, revisited. *Neurosci Lett*. 1999;266:49-52.
73. Rivera-Cervantes MC, Castañeda-Arellano R, Castro-Torres RD, Gudiño-Cabrera G, Y Velasco AI, Camins A, Beas-Zárate C. P38 MAPK Inhibition Protects Against Glutamate Neurotoxicity and Modifies NMDA and AMPA Receptor Subunit Expression. *J Mol Neurosci.* 2015;55:596-608.
74. Rojas A, Dingledine R. Ionotropic glutamate receptors: regulation by G-protein-coupled receptors. *Mol Pharmacol.* 2013;83:746-752.
75. Sakuraoka Y, Sawada T, Shiraki T, Park K, Sakurai Y, Tomosugi N, Kubota K. Analysis of hepcidin expression: in situ hybridization and quantitative polymerase chain reaction from paraffin sections. *World J Gastroenterol.* 2012;18:3727-3731.
76. Sawada K, Hosoi E, Bando M, Sakata-Haga H, Lee NS, Jeong YG, Fukui Y. Differential alterations in expressions of ryanodine receptor subtypes in cerebellar cortical neurons of an ataxic mutant, rolling mouse Nagoya. *Neuroscience.* 2008;152:609-617.
77. Sawada K, Kalam Azad A, Sakata-Haga H, Lee NS, Jeong YG, Fukui Y. Striking pattern of Purkinje cell loss in cerebellum of an ataxic mutant mouse, tottering. *Acta Neurobiol Exp (Wars).* 2009;69:138-145.
78. Sawada K, Sakata-Haga H, Fukui Y. Alternating array of tyrosine hydroxylase and heat shock protein 25 immunopositive Purkinje cell stripes in zebrin II -

defined transverse zone of the cerebellum of rolling mouse Nagoya. *Brain Res.* 2010:1343:46-53.

79. Schwaller B. Calretinin: from a "simple" Ca^{2+} buffer to a multifunctional protein implicated in many biological processes. *Front Neuroanat.* 2014;8:3.
80. Segura Torres JE, Chaparro-Huerta V, Rivera Cervantres MC, Montes-González R, Flores Soto ME, Beas-Zárate C. Neuronal cell death due to glutamate excitotocity is mediated by P38 activation in the rat cerebral cortex. *Neurosci Lett.* 2006;403:233-238.
81. Shang JL, Cheng Q, Yang WF, Zhang M, Cui Y, Wang YF. Possible roles of COX-1 in learning and memory impairment induced by traumatic brain injury in mice. *Braz J Med Biol Res.* 2014;47:1050-1056.
82. Shi WZ, Zhao CZ, Zhao B, Zheng XL, Fang SH, Lu YB, Zhang WP, Chen Z, Wei EQ. Aquaporin-4 deficiency attenuates acute lesions but aggravates delayed lesions and microgliosis after cryoinjury to mouse brain. *Neurosci Bull.* 2012;28:61-68.
83. Shohami E, Biegon A. Novel approach to the role of NMDA receptors in traumatic brain injury. *CNS Neurol Disord Drug Targets.* 2014;13:567-573.
84. Simms BA, Zamponi GW. Neuronal voltage-gated calcium channels: Structure, function, and dysfunction. *Neuron.* 2014;82:24-45.
85. Suh YS, Oda Si, Kang YH, Kim H, Rhyu IJ. Apoptotic cell death of cerebellar granule cells in rolling mouse Nagoya. *Neurosci Lett.* 2002;325:1-4.
86. Takahashi E. Cav2.1 channelopathy and mouse genetic approaches to investigate function and dysfunction of Cav2.1 channel. *In*: (Yamahuchi, M. ed.) Calcium signaling, Nova Science Publishers, Inc., New York, 2012, pp.149-158.

87. Takahashi E, Niimi K. Spatial learning deficit in aged heterozygous Cav2.1 channel mutant mice, rolling mouse Nagoya. *Exp Gerontol.* 2009;44:274-279.

88. Takahashi E, Niimi K, Itakura C. Age-related spatial and nonspatial short-term memory in Cav2.1alpha1 mutant mice, Rolling Nagoya. *Behav Brain Res.* 2009;204:241-245.

89. Takahashi E, Niimi K, Itakura C. Impairment of spatial short-term memory following acute administration of the NMDA receptor antagonist in heterozygous rolling Nagoya mice carrying the Cav2.1 alpha1 mutation. *Behav Brain Res.* 2010;213:121-125.

90. Takahashi E, Niimi K, Itakura C. Emotional behavior in heterozygous rolling mouse Nagoya Cav2.1 channel mutant mice. *Neurobiol Aging.* 2011;32:486-496.

91. Tian X, Zhou Y, Gao L, He G, Jiang W, Li W, Takahashi E. Analysis of ischemic neuronal injury in Cav2.1 channel α1 subunit mutant mice. *Biochem Biophys Res Commun.* 2013;434:60-64.

92. Tikka T, Fiebich BL, Goldsteins G, Keinanen R, Koistinaho J. Minocycline, a tetracycline derivative, is neuroprotective against excitotoxicity by inhibiting activation and proliferation of microglia. *J Neurosci.* 2001;21:2580-2588.

93. Tokuda S, Kuramoto T, Tanaka K, Kaneko S, Takeuchi IK, Sasa M, Serikawa T. The ataxic groggy rat has a missense mutation in the P/Q-type voltage-gated Ca^{2+} channel alpha1A subunit gene and exhibits absence seizures. *Brain Res.* 2007;1133:168-177.

94. Tsunekawa K, Kondo F, Okada T, Feng GG, Huang L, Ishikawa N, Okada S. Enhanced expression of WD repeat-containing protein 35 (WDR35) stimulated by domoic acid in rat hippocampus: involvement of reactive

oxygen species generation and p38 mitogen-activated protein kinase activation. *BMC Neurosci*. 2013;14:4.

95. Turner TJ, Adams ME, Dunlap K. Calcium channels coupled to glutamate release identified by omega-Aga-IVA. *Science.* 1992;258:310-313.

96. Unterberg AW, Stover J, Kress B, Kiening KL. Edema and brain trauma. *Neuroscience.* 2004;129:1021-1029.

97. Vos PE, Jacobs B, Andriessen TM, Lamers KJ, Borm GF, Beems T, Edwards M, Rosmalen CF, Vissers JL. GFAP and S100B are biomarkers of traumatic brain injury: an observational cohort study. *Neurology*. 2010;75:1786-1793.

98. Wakamori M, Yamazaki K, Matsunodaira H, Teramoto T, Tanaka I, Niidome T, Sawada K, Nishizawa Y, Sekiguchi N, Mori E, Mori Y, Imoto K. Single tottering mutations responsible for the neuropathic phenotype of the P-type calcium channel. *J Biol Chem.* 1998;273:34857-34867.

99. Watkins JC, Jane DE. The glutamate story. *Br J Pharmacol.* 2006;147 Suppl 1:S100-108.

100. Williams P, White A, Ferraro D, Clark S, Staley K, Dudek FE. The use of radiotelemetry to evaluate electrographic seizures in rats with kainate-induced epilepsy. *J Neurosci Methods.* 2006;155:39-48.

101. Xie G, Clapcote SJ, Nieman BJ, Tallerico T, Huang Y, Vukobradovic I, Cordes SP, Osborne LR, Rossant J, Sled JG, Henderson JT, Roder JC. Forward genetic screen of mouse reveals dominant missense mutation in the P/Q-type voltage-dependent calcium channel, CACNA1A. *Genes Brain Behav*. 2007;6:717-727.

102. Yang JL, Xu B, Zhang WS, Xu H, Deng XM, Zhang YQ. Gabapentin reduces CX3CL1 signaling and blocks spinal microglial activation in monoarthritic rats. *Mol Brain.* 2012a;5:18.

103. Yang XR, Sun P, Qin HP, Si PP, Sun XF, Zhang C. Involvement of MAPK pathways in NMDA-induced apoptosis of rat cortical neurons. *Sheng Li Xue Bao.* 2012b;64:609-616.

104. Yoshioka N, Hisanaga SI, Kawano H. Suppression of fibrotic scar formation promotes axonal regeneration without disturbing blood-brain barrier repair and withdrawal of leukocytes after traumatic brain injury. *J Comp Neurol.* 2010;518:3867-3881.

105. Zamponi GW, Striessnig J, Koschak A, Dolphin AC. The physiology, pathology, and pharmacology of voltage-gated Calcium channels and their future therapeutic potential. *Pharmacol Rev.* 2015;67:821-870.

106. Zhang XM, Zhu SW, Duan RS, Mohammed AH, Winblad B, Zhu J. Gender differences in susceptibility to kainic acid-induced neurodegeneration in aged C57BL/6 mice. *Neurotoxicology.* 2008;29:406-412.

107. Zwingman TA, Neumann PE, Noebels JL, Herrup K. Rocker is a new variant of the voltage-dependent calcium channel gene Cacna1a. *J Neurosci.* 2001;21:1169-1178.

Summary in Japanese

Cav2.1 チャネルの神経機能における役割に関する研究

- Cav2.1α1 遺伝子変異マウスを用いて-

電位依存性カルシウムチャネル（Cav）は神経細胞の電気的興奮を Ca^{2+}依存性の生理応答に変換する役割を担い、α1、α2/δ、β、γ サブユニットで構成される。Cav2.1 は主に中枢神経系に存在し、グルタミン酸などの神経伝達物質の放出や遺伝子発現などの神経機能の制御に関与している。グルタミン酸は中枢神経系における主要な興奮性神経伝達物質であり、記憶や学習などの高次脳機能に中心的な役割を果たしている。他方、過剰なグルタミン酸は神経が過剰に興奮するてんかんなどの原因となり、さらにはアポトーシス、壊死などを含む神経細胞障害を惹起する。グルタミン酸受容体としては、イオンチャネル内臓型の AMPA（α-amino-3-hydroxy-5-methylisoxazole-4-propionic acid）型、カイニン酸型、NMDA（N-methyl-D-aspartate）型受容体があり、また、G タンパク共役型である代謝型受容体が知られている。Cav2.1α1 サブユニット遺伝子の変異は、ヒトでは家族性片麻痺性偏頭痛 1 型、脊髄小脳性失調症 6 型、反復発作性失調症 2 型、特発性全般てんかんなどの原因として報告されている。実験動物としては複数の Cav2.1α1 変異マウスが系統化されており、運動失調、てんかん、記憶障害などを示すが、それらの症状並びに表現型は様々である。

本研究では、Cav2.1 チャネルの神経機能における役割を解明する目的で、以下の異なる２系統の Cav2.1α1 変異マウスを用いて実験を行った。一つは

Cav2.1α1 遺伝子内に変異がある *rolling Nagoya* マウスを用いて、カイニン酸誘発性てんかんの感受性や神経細胞変性への抵抗性について検索した。他の一つは新規に Cav2.1α1 遺伝子変異マウスとして見出された *tottering-6j* マウスを用いて、てんかんや小脳における遺伝子発現について調べた。

Rolling Nagoya マウスは、Cav2.1α1 サブユニットのドメイン III 内の電位センサーS4 領域内に変異があるため電位感受性が野生型より 40%低下し、運動機能障害を示すが、てんかん発作は示さない常染色体劣性の系統である。この一見正常なヘテロマウスでは、加齢依存的に変異型 Cav2.1α1 サブユニット遺伝子の発現が上昇し、野生型マウスに比べカイニン酸投与によるてんかん発作は加齢依存的に抵抗性を示した。これの組織病理学的解析からは、海馬 CA1 および CA3 において変性錐体細胞並びに反応性アストロサイトの減少が認められ、ウエスタンブロット法ではリン酸化 p38 の発現の減少が認められた（１章)。また、このホモマウスに凍結脳損傷を起こして解析した結果、野生型マウスに比べ損傷領域における変性神経細胞並びに反応性アストロサイトの減少が損傷後 1 日目および 7 日目で認められ、ウエスタンブロット法によりリン酸化 p38 の発現が減少していた（２章)。*Rolling Nagoya* マウスを用いたこれらの結果から、Cav2.1 チャネル依存性 p38 シグナルカスケードは、カイニン酸誘発性てんかん並びに神経細胞変性への抵抗性に関与していることが示された。

Tottering-6j マウスは Cav2.1α1 サブユニットのドメイン I 内の S4 から S6 の領域が一部欠損した運動機能障害を示す常染色体劣性の系統である。これのホモマウスを電気生理学的並びに薬理学的に解析した結果、これの薬理学的

な特徴としては、このマウスはヒトに類似した欠神発作を示すことが明らかになった。小脳では野生型マウスに比べ tyrosine hydroxylase、zebrin II、ryanodine receptor 3 の発現が高く、calretinin の発現が低くかった（３章)。以上の結果から、*tottering-6j* マウスはヒトの欠神性発作の疾患モデル動物になること、小脳における遺伝子発現機能に Cav2.1 チャネルを介した Ca^{2+}シグナリングが関与していることが示唆された。

Rolling Nagoya マウスを用いた本研究により、Cav2.1 チャネルは p38 シグナルカスケードを介した神経細胞の保護作用に関与していることが明らかとなった。また、Cav2.1 チャネル阻害剤や p38 リン酸化阻害剤はてんかんや脳損傷に対する治療剤として有用である可能性が示唆された。他方、*tottering-6j* マウスを用いた研究によっては、Cav2.1 チャネルの変異部位の違いによる機能変化は、てんかんの発症に影響を与えること、小脳における遺伝子発現には Cav2.1 チャネルを介したシグナル伝達経路が関与していることが明らかとなった。よって *tottering-6j* マウスは、Cav2.1 チャネルの機能解析に有用なモデル動物であることが示唆された。さらに本研究からは、Cav2.1α1 サブユニット遺伝子の変異によって表現型が異なるのは、その変異部位の違いによってチャネル機能に異なる変化を起こし、中枢神経系機能を支えている複雑な神経回路ネットワークの制御を多様に乱すことが示唆された。